frontiers | Frontiers in Earth Science

TYPE Original Research
PUBLISHED 03 June 2024
DOI 10.3389/feart.2024.1363029

OPEN ACCESS

EDITED BY
Jaroslaw Majka,
Uppsala University, Sweden

REVIEWED BY
Anna Pietranik,
University of Wrocław, Poland
Igor Broska,
Slovak Academy of Sciences, Slovakia

*CORRESPONDENCE
Fazilat Yousefi,
fazilat.yousefi@unb.ca

RECEIVED 29 December 2023
ACCEPTED 16 April 2024
PUBLISHED 03 June 2024

CITATION
Yousefi F, Lentz DR, McFarlane CRM, Walker JA and Thorne KG (2024), Zircon compositional systematics from Devonian oxidized I-type granitoids: examination of porphyry Cu fertility indices in the New Brunswick Appalachians, Canada. *Front. Earth Sci.* 12:1363029. doi: 10.3389/feart.2024.1363029

Zircon compositional systematics from Devonian oxidized I-type granitoids: examination of porphyry Cu fertility indices in the New Brunswick Appalachians, Canada

Fazilat Yousefi[1]*, David R. Lentz[1], Christopher R. M. McFarlane[1], James A. Walker[2] and Kathleen G. Thorne[3]

[1]Department of Earth Sciences, University of New Brunswick, Fredericton, NB, Canada, [2]Geological Surveys Branch, Department of Natural Resources and Energy Development, Bathurst, NB, Canada, [3]Geological Surveys Branch, Department of Natural Resources and Energy Development, Fredericton, NB, Canada

Zircon is a common, widely distributed accessory mineral in most igneous rocks and its refractory nature records magmatic evolution in terms of oxygen and U-Th-Pb isotopes, and trace-element contents all of which reflect the intrinsic physio-chemical evolution of the magmatic systems in which it crystallized. Zircon compositions can be used as an indicator of relative fertility of hypabyssal intrusions in terms Cu ± Mo ± Au porphyry mineralization. To further characterize syn- to post-collisional adakitic Devonian oxidized I-type granitoids in the New Brunswick (specifically, those with Cu ± Mo ± Au porphyry-style mineralization), LA-ICP-MS analyses (guided by μXRF-EDS mapping and SEM-BSE imaging of polished thin sections) of zircons from 13 granitoids was conducted. The zircons studied were similar in terms of their textures (homogenous cores, patchy zoning, oscillatory zoning, and some unzoned zircon); however, they have a wide range of trace- and minor-element (Hf, HREE, Y, Th, U) compositions. Specifically, Zr/Hf ranges between 24–60, whereas Th/U ranges between 0.15 and 5.37. The presence of inherited zircon affects the concentrations of Th and U, as well as other key elements. Estimated crystallization temperatures of granitoids, ranging from 737 to 899°C, were calculated via Ti-in-zircon geothermometry assuming reduced TiO_2 and SiO_2 activities. The calculated log fO_2 values for zircons from some of these granitoids indicate a highly oxidized magmatic signature. Zr/Hf, Eu/Eu*, and (Eu/Eu*)/Y in zircon, as well as zircon (Ce/Nd)/Y are some of the best indicators of porphyry fertility. The Ce/Ce* in zircon exhibit a large range (1.1–590), with higher Ce/Ce* reflecting more metallogenically favourable oxidizing conditions. If Eu/Eu* in zircon is ≥0.4 (relatively oxidized conditions), it indicates a high potential for an ore-forming porphyry Cu mineralizing system. Lower Eu contents reflect relatively reducing conditions, as Eu anomalies vary with oxygen fugacity as well, and the relative abundance of Eu^{2+} is higher, but does not substitute into the zircon lattice. The evidence extracted from analyzing the zircon

composition within New Brunswick's I-type granitoids indicates the fertility of these hypabyssal intrusions.

KEYWORDS

Zircon chemistry, oxidized I-type, porphyry Cu fertility, New Brunswick, Appalachians, Eu anomaly

1 Introduction

Hypabyssal felsic intrusions are commonly associated with significant Cu-bearing magmatic hydrothermal systems (Sillitoe, 2010; Sun et al., 2015). Porphyry copper (± Mo ± Au) deposits constitute roughly 20%, 50%, and 75% of the global gold, molybdenum, and copper resources, respectively. Critically, all the world's molybdenum reserves are attributed to porphyry-type deposits, and most of the Re, as well as minor amounts of other metals, such as Ag, Pd, Te, Se, Bi, Zn, and Pb (Sillitoe, 2010). Metal contents and petrogenetic associations of porphyry deposits are quite diverse. Porphyry deposits are typically large, low- to medium-grade deposits; they are spatially and genetically associated with felsic and intermediate porphyritic intrusions (Sinclair, 2007). There are many intrusive rocks in the northern part of Appalachian orogenic belt (in USA and Canada) that are associated with various mineralization types, including porphyry Cu±Mo±Au (Hollister et al., 1974). Cu, Mo, and Au porphyry deposits in the northern Appalachians, including New Brunswick (NB), occur over a wide time span, although are predominantly Devonian in age (Yousefi et al., 2022b).

Porphyry indicator minerals (PIMs), such as zircon, plagioclase, apatite, magnetite, epidote, chlorite, and tourmaline (cf. Cooke et al., 2020) can be useful in assessing the fertility and evolution of magmatic hydrothermal systems. According to Bacon (1989), accessory minerals may nucleate near the host crystal/liquid interface because of local saturation owing to formation of a differentiated chemical boundary layer in which accessory mineral solubility would be lower than in the surrounding liquid. In particular, zircon has been receiving considerable attention in recent years. Its refractory nature and very low diffusion coefficients of tetravalent cations minimize the intracrystalline diffusion-controlled redistribution of isomorphic components, thereby making it one of the most reliable monitors of evolving magmatic processes (Aranovich and Bortnikov, 2018). Zircon is commonly present in felsic to intermediate igneous rocks, and can record the compositional properties of the parent magma, controlled by the relevant zircon/melt partition coefficients of each element, it has received notable attention in recent years (cf. Dilles et al., 2015). Zircon is robust and can survive post-crystallization processes like weathering, transportation, diagenesis, metamorphism, and even crustal melting (Luo and Ayers, 2009). The geochemistry of zircon presents an opportunity to better understand the genesis of and pathfinders for large magmatic-hydrothermal ore systems (Courtney-Davies et al., 2019). According to Cooke et al. (2020), the intermediate to felsic intrusive complexes that produce porphyry Cu deposits typically contain zircon as a magmatic accessory phase. Zircon is the most robust high temperature geochronometer available for magmatic rocks, and can provide a deep understanding of magma genesis by using radiogenic and O-isotopic and trace-element compositional systematics. In porphyry systems, the hydrothermal fluids responsible for ore formation are commonly associated with calc-alkaline, silicic magmatic intrusions (Burnham, 1979).

Assessing the fertility of intrusions and potential hydrothermal alteration zones in New Brunswick (NB) through the analysis of zircons within these intrusive suites is essential for uncovering new resource opportunities. Studied zircons of Devonian oxidized I-type granodiorites of New Brunswick (NB) are from Eagle Lake Granite (ELG) associated with porphyry Cu±Mo occurrence; Blue Mountain Granodiorite Suite associated with porphyry Cu±Mo occurrence; Evandale Granodiorite associated with porphyry Cu±Mo±Au occurrence, Sorrel Ridge Granite associated with porphyry Cu±Mo occurrence, Magaguadavic Granite associated with porphyry Cu±Mo±Au occurrence, Popelogan Granodiorite associated with porphyry Cu occurrence, Dawson (McQuirks) Mtn associated with porphyry Cu occurrence, Red Brook Granodiorite associated with porphyry Cu±Mo occurrence, Falls Creek Granodiorite associated with porphyry Cu±Mo occurrence, Nicholas Denys Granodiorite associated with porphyry Cu±Mo occurrence, McKenzie Gulch Porphyry associated with porphyry Cu±Mo occurrence, Rivière Verte Porphyry associated with porphyry Cu±Mo occurrence, Watson Brook Granodiorite associated with porphyry Cu±Mo occurrence, and Sugarloaf Mountain (no specific mineralization).

The most important information obtained from the geochemistry of zircons includes investigation of Ce and Eu anomalies in oxidized magma, calculation of zircon crystallization temperature, and looking at variation of Zr/Hf, U, Th, and REE patterns as evidence of magma evolution (Kemp et al., 2007; Cooke et al., 2020). Also, magmatic zircon commonly accommodates minor and trace amounts of lithophile elements, such as Sc, Y, the rare earth elements (REE), Ti, Hf, Th, U, Nb, Ta, V, and P in crustal felsic igneous rocks (see Luo and Ayers, 2009). According to Azadbakht et al. (2018), plagioclase, K-feldspar, monazite, xenotime, zircon, and apatite are common REE-bearing minerals in these felsic I-type granodiorites in NB. In this study, we report LA-ICP-MS analysis of trace-element compositions of zircons collected from 13 porphyry systems in NB associated with Cu±Mo±Au mineralization. Also, we used zircons in Devonian oxidized I-type granitoids in NB as a porphyry indicator mineral (PIMs) to investigate the fertility (or infertility) of these porphyritic intrusions; it is considered as a main focus of this manuscript. The oxidized nature of these specialized I-type granitoids, previously discussed (Yousefi et al., 2022), has been confirmed in NB. Peraluminous I-type granitoids in NB have been confirmed with the $Al_2O_3/(CaO+Na_2O+K_2O)$ ratio (1.0–1.3) (Azadbakht et al., 2019; Yousefi et al., 2023a), reflecting their mineralogy. Additionally, based on research by Yousefi et al. (2023c)

and by using $FeO^*/(FeO^* + MgO)$ vs. SiO_2 diagram (Frost et al., 2001) for NB granitoids, the samples plot as magnesian granites, which typically reflect oxidized I-type granites.

2 Geological setting

In the northern Appalachians, the temporal and spatial distribution of granitoids and related mineralization are controlled by the tectonic history of the orogen, specifically the regional to local structural features (Kellett et al., 2021). According to Ruitenberg et al. (1977) and Ruitenberg and Fyffe (1982), Acadian and post-Acadian mineral deposits in southern NB are correlated with a distinct sequence of tectonic events with a significant variety of epigenetic deposits occurring in and along the contacts of Middle Devonian to Early Carboniferous igneous intrusions and associated subvolcanic stocks emplaced in extension structures. It is important not to overlook the contributions of transpression and transtension in aiding the rise and placement of magma, which forms these zircons that are host intrusive rocks in NB.

The 13 late-to post-tectonic, Early to Late Devonian, oxidized I-type intrusions investigated are within the northern Canadian Appalachians, part of the Appalachians-Caledonian Mountain belt, which it is considered as one of the Earth's classic orogens (van Staal and Barr, 2012) (Figure 1). According to van Staal and Barr (2012), the Canadian Appalachians contain a complex tectonic combination of mainly Early Paleozoic suprasubduction zone oceanic and ribbon-shaped microcontinental terranes, which were accreted to Laurentia during Early to Late Paleozoic closure of the Iapetus and Rheic oceans; during this period, the Laurentian margin gradually expanded oceanward during the successive accretion of eight litho-tectonic terranes, i.e. 1) Popelogan, 2) Elmtree, 3) Miramichi, 4) St. Croix, 5) Annidale, 6) New River, 7) Brookville, 8) Caledonia (Fyffe et al., 2011), and are included in the Dunnage, Gander and Avalon tectonic zones of the Appalachians (Hibbard et al., 2006); most of these zircons are hosted within oxidized I-type granitoids that are concentrated in Avalon, Gander, and Dunnage zones.

The oxidized I-type Devonian intermediate to felsic intrusions (hosting the studied zircons) investigated occur throughout NB are the Sorrel Ridge Granite (378.1 Ma, U-Pb zircon. Late Devonian), Magaguadavic Granite (403 ± 2 Ma, U-Pb zircon, Early Devonian), Eagle Lake Granite (ELG) (360 ± 5 Ma, U-Pb zircon, Late Devonian), Evandale Granodiorite (390.4 Ma, U-Pb zircon, Middle Devonian), and Dawson (McQuirks) Mtn (undated) in south and southwestern NB and the Blue Mountain Granodiorite Suite (BMGS) (400.7 ± 0.4 Ma, U-Pb zircon, Early Devonian), Popelogan Granodiorite (390 ± 2.3 Ma, U-Pb titanite, Middle Devonian), Falls Creek Granodiorite (undated), Nicholas Denys Granodiorite (381 ± 4 Ma, U-Pb zircon, Late Devonian), Red Brook Granodiorite (383 ± 1/-3 Ma, U-Pb zircon, Late Devonian), Rivière Verte Porphyry (368 ± 2 Ma, U-Pb zircon, Late Devonian), Watson Brook Granodiorite (undated), Sugarloaf Mountain (undated), and McKenzie Gulch Porphyry/Dyke swarm (386.2 ± 3.1 and 386.4 ± 3.3 Ma, U-Pb zircon, Late Devonian) in central and northern NB. The Early to Late Devonian ages of most of these intrusions was confirmed in previous studies (Yousefi et al., 2023d, 2022, 2021) and is consistent with emplacement during the latter stage of, and immediately after, the Acadian Orogeny. Based on geochemical characteristics (metaluminous or peraluminous, reduced/oxidized I-type and S-type, fractionated or unfractionated), Azadbakht et al. (2019) categorized these granitoids into three groups: NB-1, NB-2, and NB-3. Our research was focused on NB-1 and NB-2 (I-type granitoids). Azadbakht et al. (2019) mentioned that these granitoids formed prior to the main phase of Acadian deformation/metamorphism, although they truncate Acadian folding. The genesis of these three groups is described as follows: NB-1 granites are formed by partial melting of the lower crust, whereas NB-2 granites are formed by varying degrees of partial melting of a mixed mantle-older crustal protolith. The distinct geochemical variations observed within the subgroups of NB-1 and NB-2 can be explained by varying levels of assimilation fractional crystallization and secondary hydrothermal alteration (Azadbakht et al., 2019). Also, the NB-3 granites are predominantly derived from crustal sources and are linked to processes of Late Devonian crustal thinning associated with crustal delamination following the juxtaposition of diverse crustal blocks.

Other investigations into NB granitoids (Whalen, 1993, 1996b, 1998; Whalen et al., 1994a, b) provide insight on the petrogenesis of the intrusions hosting the zircons investigated in this study, and their relationships to mineralization. Based on radiogenic Sr isotopic work (Whalen, 1993; Whalen et al., 1994b; 1996b; 1998; Azadbakht et al., 2016; Mohammadi et al., 2017), Group NB-1 granites have initial $^{87}Sr/^{86}Sr$ values ranging from 0.703 to 0.707 and imply a mantle or juvenile crustal (I-type granite) source with a partial component of older crust. Group NB-2 granites have higher $^{87}Sr/^{86}Sr$ (>0.705) relative to group NB-1 reflecting a greater contribution of crustal material; these results are also supported by Nd isotopic signatures. According to Azadbakht et al. (2019), group NB-1 granites, except for the Magaguadavic Granite, have negative ε_{Nd} values that are interpreted to reflect contribution of older continental crust or an enriched mantle source. Group NB-2 has a larger range of ε_{Nd} (−3.4 to +2.20), which implies different degrees of mantle-crust interactions. Based on Whalen et al. (1996a) and Azadbakht et al. (2019), some of the granites assigned to group NB-2 occur on the border of Gander-Avalon border and have a wider range of $\varepsilon_{Nd,}$ likely reflecting contributions from more than one continental basement blocks. According to Whalen and Hildebrand (2019), host intrusions characterized by lower levels of Nb, Ta, Nb+Y, and Ta+Yb, and higher concentrations of La, Sm, Gd, and Nd suggest an origin related to slab failure. The theory of slab break-off concerning the origin of New Brunswick's Devonian I-type granitoids (hypabyssal) is referenced by Yousefi et al. (2024).

3 Analytical techniques

Nineteen polished thin sections from 13 hypabyssal Devonian I-type intrusions were prepared in the rock preparation laboratory of the Earth Science Department at the University of New Brunswick, Canada. In preparation for laser ablation-inductively coupled plasma-mass spectrometry (LA-ICP-MS) analysis of zircons, the polished thin sections were scanned with the M4 Tornado μ-XRF to produce Energy Dispersive Spectrometry (EDS) elemental maps to aid zircon location for follow-up analysis. High resolution backscattered electron (BSE) images of zircon were taken using the

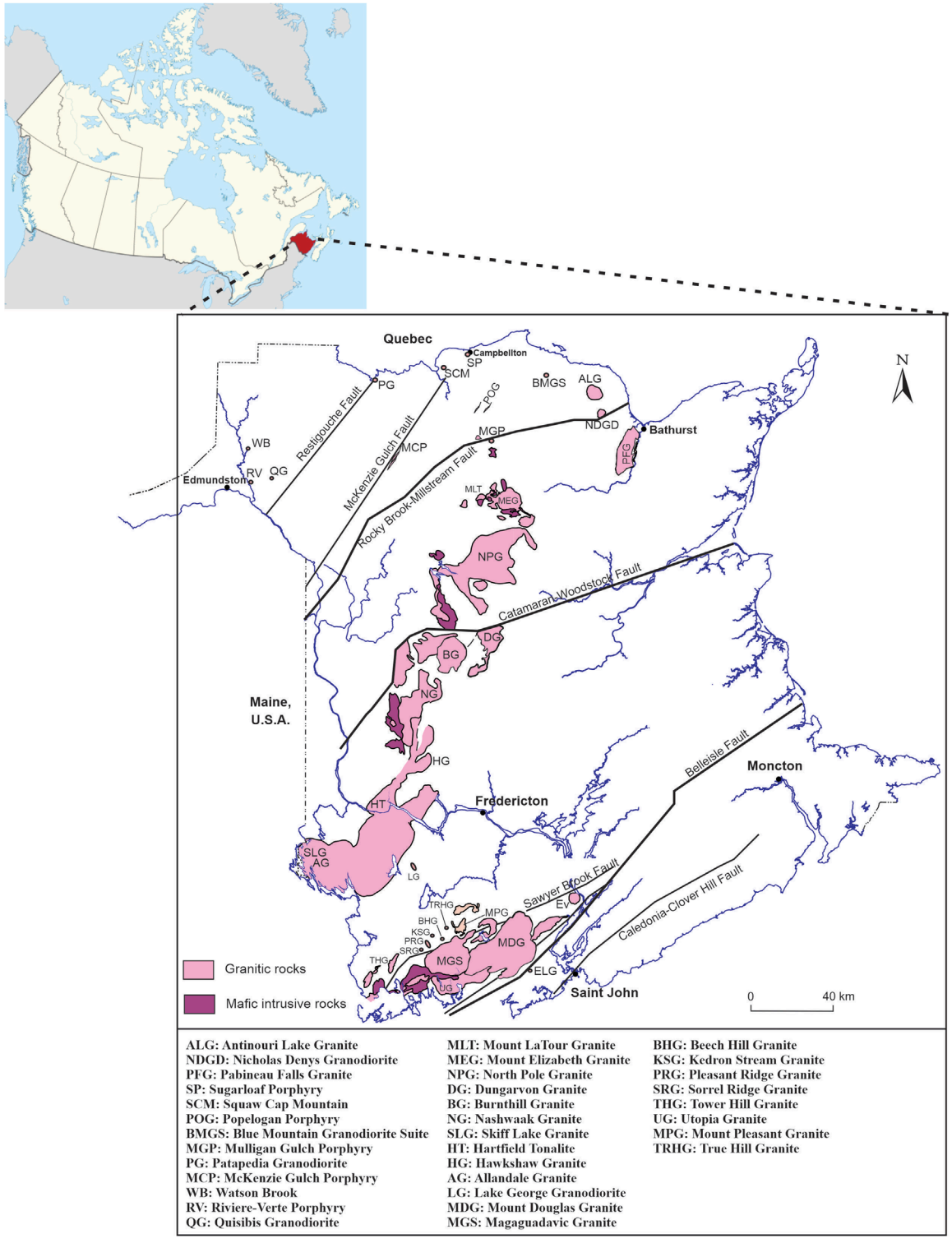

FIGURE 1
Lithological map of New Brunswick, showing location of Early to Middle and Late Devonian granitoids in NB (modified after Fyffe et al., 2008).

JEOL 6400 SEM in the University of New Brunswick Microscopy and Microanalysis facility to select suitable zircon grains for LA-ICP-MS analysis. Ablation was conducted using Resonetics S-155-LR 193 nm ArF Excimer laser ablation system coupled to an Agilent 8,900 Triple Quadrupole ICP-MS. We used a 17-um spot, 3 J/cm^2, a laser firing rate of 3 Hz. Gas flows were 900 mL/min of Argon, 300 mL/min for ultra-pure Helium, and 2 mL/min for ultra-pure nitrogen. Standard reference materials NIST 610, NIST 612, Zircon 91,500, and Zircon Plesovice were used to test the precision and accuracy of analyses.

Temperature estimations for zircon crystallization in the examined I-type granitoids were determined utilizing the Ti-in-zircon geothermometer, with adjustments made for decreased TiO_2 and SiO_2 activities (Hanchar and Watson, 2003): log(Ti ppm) = 5.711 ± 0.072–4,800 (±86)/T (K)- $\log(a_{SiO_2})$ + $\log(a_{TiO_2})$. The activity of TiO_2 is acceptable around 0.5, at which, the activity of silica for crystallization of zircon is approximately 1 (Hayden and Watson, 2007; Schiller and Finger, 2019). Following the procedure outlined by Smythe and Brenan (2016) and utilizing an Excel spreadsheet for calculating and estimating the $\log fO_2$ of the melt during zircon crystallization, we employed the bulk geochemical composition of Watson Brook Granodiorite, Magaguadavic Granite, ELG, Nicholas Denys Granodiorite, BMGS, and Rivière Verte Porphyry, for which their geochemical data were available. Additionally, the average trace element concentration of their zircons is considered in this method. The $\log fO_2$ of the NB granitoids samples is determined following the methodology outlined in Smythe and Brenan (2016). It is computed using the equation: $\log fO_2$ (sample)–$\log fO_2$ (FMQ) = 3.998 (±0.124) $\log[Ce/\sqrt{(U^* Ti)^2}]$ + 2.28 (±0.10).

4 Results

4.1 EDS and SEM-BSE images

After petrographic studies and polished thin section scanning by M4 Tornado μ-XRF to produce EDS elemental maps, the location of zircons in these porphyry rocks were precisely determined to facilitate other micro-analytical work (Figure 2). SEM-BSE images of zircon were taken using the JEOL 6400 SEM in the University of New Brunswick Microscopy and Microanalysis facility to select suitable zircon grains for LA-ICP-MS analysis (Figure 3). As can be seen from the SEM-BSE images (Figure 3), zircon grains range between 10 and 90 μm in long direction and display a variety of textures such as oscillatory zoning, and homogenous cores. The zircons investigated are generally euhedral to subhedral (Figures 3A—F). In the following explanation of zircon images, high and low BSE intensity domains are referred to as 'U-Th-Y-rich' and 'U-Th-Y-poor', respectively. In Figures 3B, G, I–KL, Q, and P, oscillatory growth zoning, with oscillatory zones of variable width are common. The bright parts of zircon in the BSE images are enriched in some elements, such as REE-U-Th and Y in comparison to the darker zones (Fowler et al., 2002). In specific circumstances, the growth of crystals can change its immediate surroundings and thus impact its own growth conditions. This feedback mechanism gives rise to nonlinearities, which can trigger the spontaneous formation of chemical oscillatory patterns (e.g., zoning). Variation and oscillations in trace-element chemistry among the zones in oscillatory zoning exist (Halden et al., 1993). Halden et al. (1993) also mention ways of generating such zones; 1) oscillatory changes in partition coefficients corresponding to temperature fluctuations, 2) repeated injection of new liquids with mixing and new growth, and 3) variation in rate of crystal growth. Oscillatory zoning shows how a feedback mechanism involving varying rates of component diffusion to the crystal's surface influences the development of different zones within the growing crystal, and diffusion and substitution on a small scale affects for forming these type of zonings (Halden et al., 1993). Homogeneous zircon cores are seen in most of these studied zircons and some of these homogeneous unzoned cores surrounded by oscillatory zoning. The homogeneous and unzoned core of the crystal indicates that it initially formed under nearly equilibrium conditions (Fowler et al., 2002). The next texture that is characterized here is patchy zoning, which reflects bimodal chemical distribution, representing the predominant textural type in zircon core (Figures 3H,I,K) and this often involves U-Th-Y-poor zircon gradually replacing U-Th-Y-rich zircon to different degrees. This texture is attributed to complex coupled dissolution reprecipitation process (CDRP) and may continue until complete replacement of the U-Th-Y-rich core (cf. Gagnevin et al., 2010). According to Tramm et al. (2021), the patchy zoning observed in zircon, which persists down to submicron scales, is attributed to metamictization and annealing effects primarily by temperature driven diffusion reactions.

In some U, Th, and Y rich homogeneous cores are mantled by a zone of resorption and oscillatory zoning marked by decreased U, Th, and Y contents (Figures 3A, E). Some of the zircons investigated (Figure 3D, M, O, and R) do not display any zoning or have only weakly developed zoning with low U-Th-Y contents.

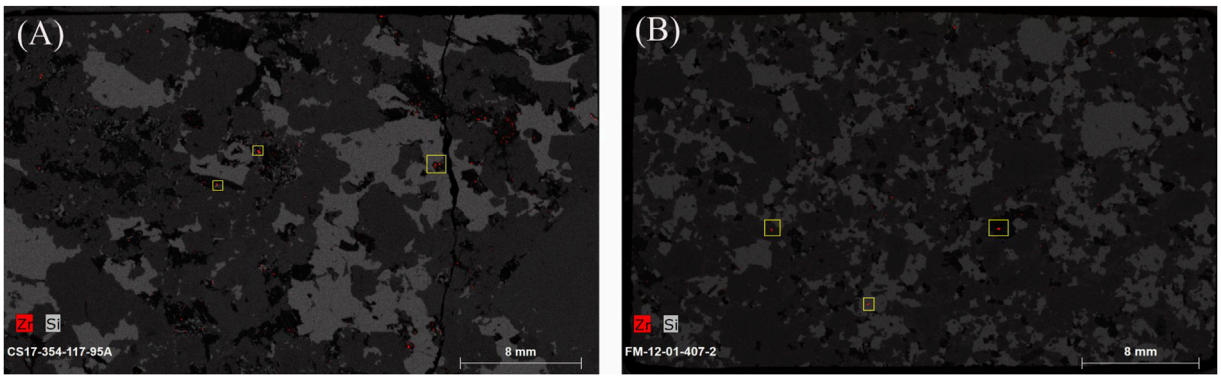

FIGURE 2
(A, B) MicroX-ray Fluorescence–Energy Dispersive Spectrometry (μXRF-EDS) chemical maps that demonstrate zircon (red) and silica (gray) coexistence in two example samples CS17-354-117.95A (Magaguadavic Granite) and FM-12–01-407.2 (Nicholas Denys Granodiorite).

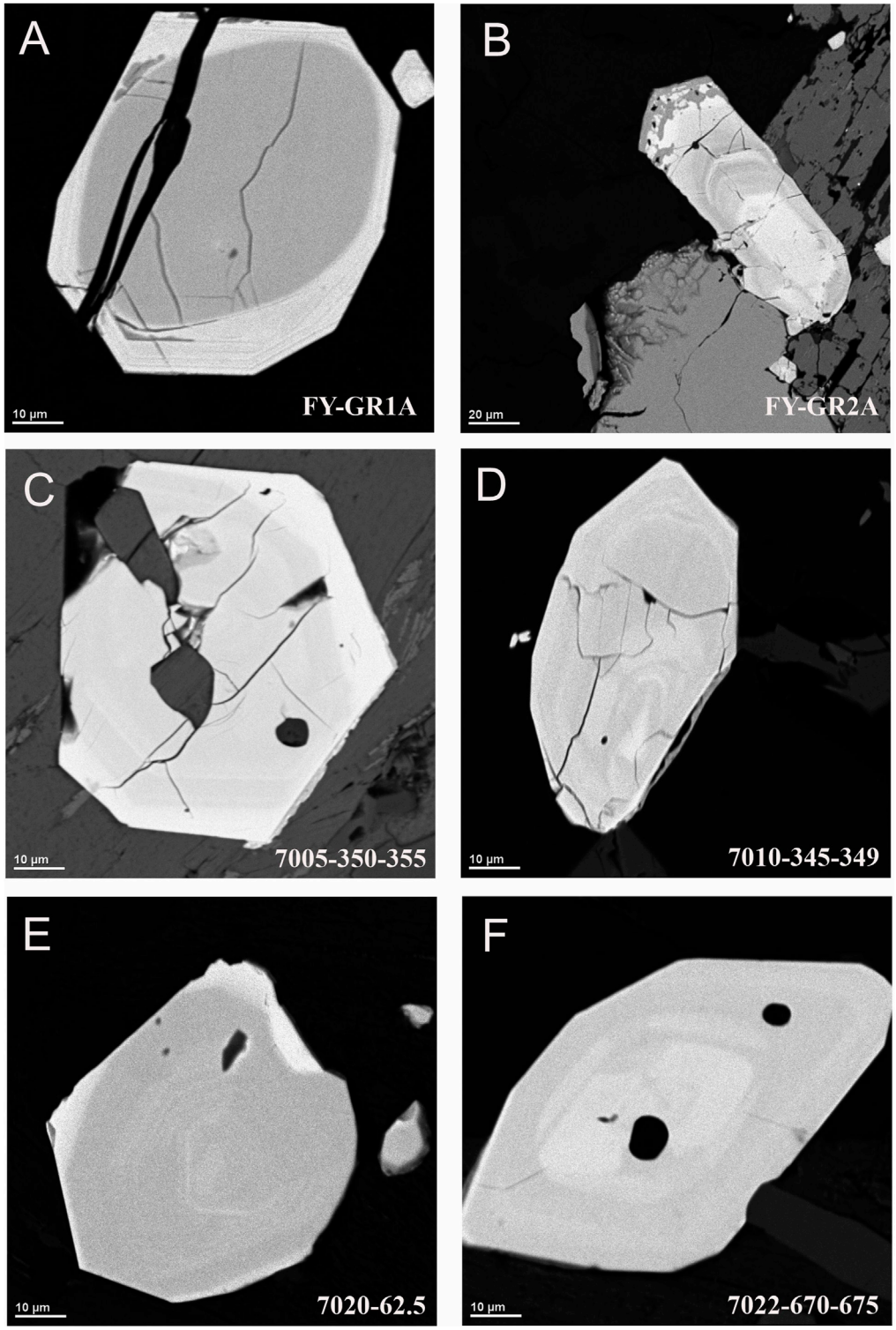

FIGURE 3
(Continued).

4.2 LA-ICP-MS

Table 1 presents the average trace-element concentrations of 44 zircons from 13 hypabyssal Devonian I-type intrusions in NB, including Ca, Sc, Ti, Y, Zr, Nb, La, Ce, Pr, Nd, Sm, Eu, Gd, Tb, Dy, Ho, Er, Tm, Yb, Lu, Hf, Ta, Pb, Th, U, while the Supplementary Material contains the raw data. The REE patterns of magmatic zircons from oxidized I-type granitoids examined in this

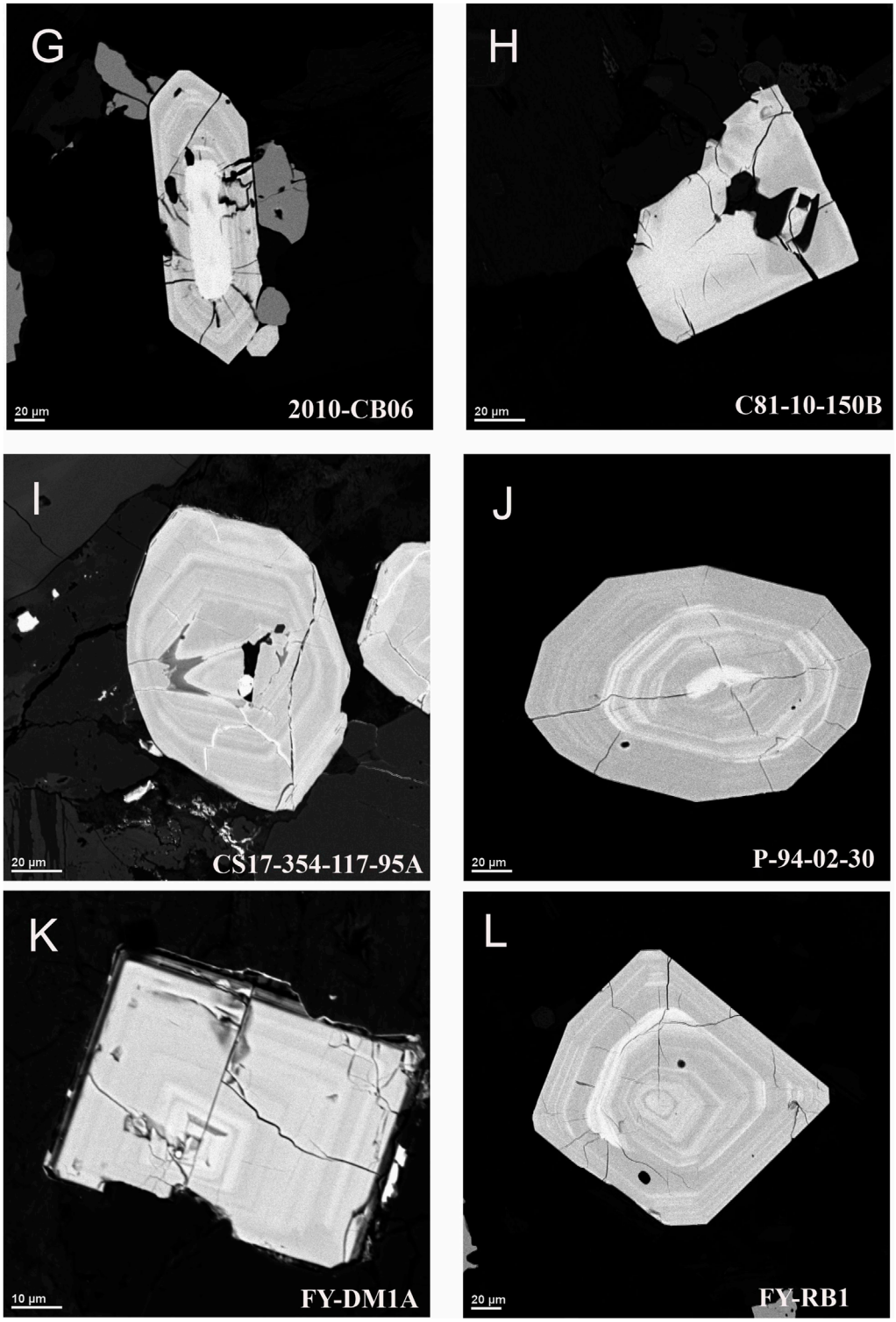

FIGURE 3
(Continued).

study are presented in Figure 4. Relatively low to strong negative Eu anomalies, and positive Ce anomalies, and depletion of LREE relative to HREE are observed in all the magmatic zircons from these intrusions.

4.3 Ti-in-zircon thermometry

The Ti-in-zircon thermometer is based on the temperature-dependent exchange reaction (Fu et al., 2008): $ZrSiO_4 + TiO_2 =$

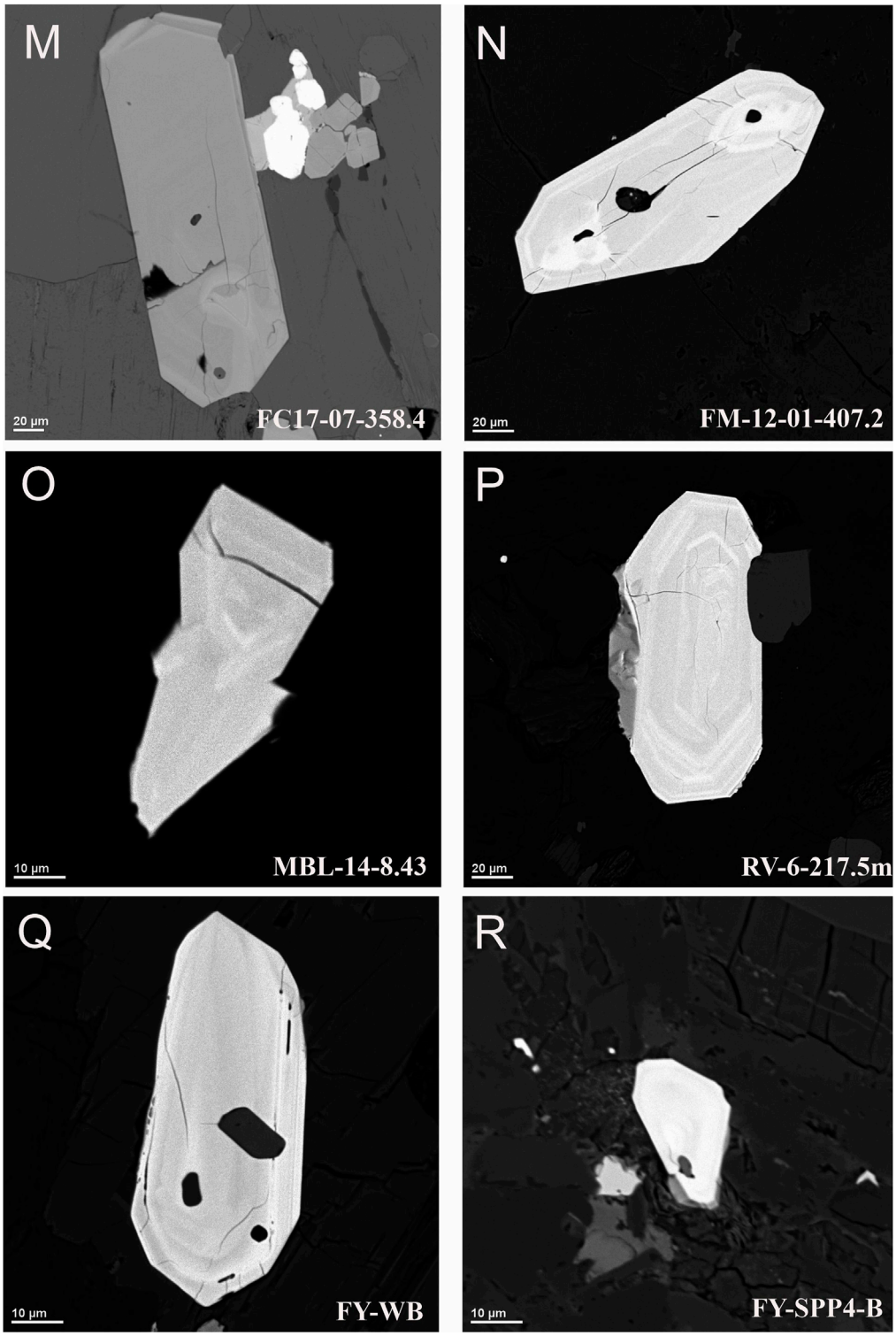

FIGURE 3
(Continued). SEM-Backscattered electron images (SEM-BSE) showing textures observed in zircons from granitoids examined during this study. The numbers in the corner of the figures are the numbers of the samples and the numbers of the drill cores used. **(A, B)** Eagle Lake Granite (ELG) associated with porphyry Cu±Mo deposits; **(C-F)** Blue Mountain Granodiorite Suite associated with porphyry Cu±Mo deposit (BMGS); **(G)** Evandale Granodiorite associated with porphyry Cu±Mo (Au) deposit; **(H)** Sorrel Ridge Granite associated with porphyry Cu±Mo deposit; **(I)** Magaguadavic Granite associated with porphyry Cu±Mo±Au deposit; **(J)** Popelogan granodiorite associated with porphyry Cu deposit; **(K)** Dawson (McQuirks) Mtn associated with porphyry Cu deposit; **(L)** Red Brook Granodiorite associated with porphyry Cu±Mo deposit; **(M)** Falls Creek Granodiorite associated with Cu±Mo deposit; **(N)** Nicholas Denys Granodiorite associated with Cu±Mo deposit; **(O)** McKenzie Gulch porphyry associated with porphyry Cu±Mo deposit; **(P)** Rivière Verte Porphyry associated with porphyry Cu±Mo deposit; **(Q)** Watson Brook Granodiorite associated with porphyry Cu±Mo deposit; and **(R)** Sugarloaf Mountain.

10.3389/feart.2024.1363029

TABLE 1 Average LA-ICP-MS trace element data (ppm) of zircons from oxidized I-type granite in New Brunswick.

Samples	1	2	3	4	5	6	7	8	9	10	11	12	13
Ti	109.6	84.4	73.7	6.0	6.3	22.4	5.5	5.9	5.1	8.2	9.6	9.9	23.5
Sc	364.7	433.3	330.8	288.4	259.8	320.1	256.2	264.8	340.3	309.2	275.7	379.8	250.5
Y	830.5	2444.3	986.9	792.4	935.1	2915.8	1827.5	1538.5	877.5	1139.1	1412.3	1333.3	1432.6
Zr	419047	398504	425929	424126	407006	425284	433814	422994	429562	424091	440591	446287	423627
Hf	8351	11151	8685	8841	9594	8417	10166	8626	9107	8847	9923	8250	8746
Zr/Hf	102	35	49	47	42	50	42	49	47	47	44	54	48
Nb	1.4	69.9	1.9	2.4	4.5	76.1	10.1	2.8	1.9	2.5	28.1	3.1	1.7
Ta	0.44	10.94	0.58	0.77	1.29	6.82	4.34	0.94	0.55	0.92	2.14	0.92	0.84
Nb/Ta	3.18	6.38	3.27	3.11	3.48	11.15	2.32	2.97	3.45	2.71	13.13	3.36	2.02
Pb	4.11	35.78	7.64	10.22	16.72	23.05	26.91	29.74	5.04	22.97	10.03	7.46	29.98
Th	97.93	645.63	218.12	792.09	568.49	724.98	488.58	674.56	127.19	173.91	160.72	212.39	803.41
U	145	1593	510	306	1022	350	960	503	208	323	379	292	373
Th/U	0.67	0.40	0.42	2.58	0.55	0.07	0.50	1.34	0.61	0.53	0.42	0.72	2.15
Eu/Eu^*	0.51	0.46	0.54	0.59	0.41	0.03	0.12	0.46	0.62	0.35	0.14	0.46	0.40
Ce/Ce^*	71.03	60.34	40.59	197.33	99.16	12.35	24.05	6.27	55.00	41.13	2.50	7.10	15.65
La	0.15	3.35	0.27	10.08	22.59	0.49	0.62	2.22	0.05	6.24	3.18	0.49	2.47
Ce	13.90	56.33	20.08	41.67	120.41	34.02	37.31	51.03	19.88	24.77	19.70	22.24	69.21
Pr	0.16	3.55	0.16	1.13	11.44	1.13	0.49	0.85	0.11	0.86	1.29	1.15	1.55
Nd	1.9	18.31	2.01	5.62	60.39	13.19	4.47	8.06	1.68	4.89	9.12	12.49	13.33
Sm	3.6	15.25	3.43	3.86	17.57	21.09	6.85	10.27	3.54	4.38	8.64	10.70	14.04
Eu	1.44	4.02	1.52	1.47	3.09	0.45	0.61	3.19	1.77	1.22	0.93	3.03	3.47
Gd	21.23	50.76	21.33	16.46	30.51	96.47	35.10	42.90	20.19	23.80	36.11	38.22	51.41
Tb	6.45	18.79	6.93	5.18	7.59	28.36	12.72	12.49	6.23	7.93	11.89	11.22	13.43
Dy	72.26	236.04	84.27	64.08	84.77	317.28	161.78	142.03	75.06	98.34	139.04	122.85	139.61
Ho	27.03	85.48	31.69	24.75	30.01	106.75	60.49	49.24	27.77	37.24	48.20	43.86	46.62
Er	125.74	415.87	153.45	125.01	144.64	464.40	259.44	229.54	134.01	181.91	221.21	199.78	207.61
Tm	24.75	86.11	31.74	26.92	30.22	85.70	61.87	46.42	27.73	37.22	42.66	39.14	39.98
Yb	219.96	777.29	295.68	263.26	285.88	718.12	557.94	418.01	259.25	342.08	364.46	344.38	343.92
Lu	46.66	153.36	64.09	58.92	61.42	138.35	109.84	86.11	56.79	71.73	69.47	70.36	68.02

Note: Samples are listed by numbers. These numbers represent these areas: 1: Blue Mountain Granodiorite Suite, 2: Eagle Lake Granite, 3: Red Brook Granodiorite, 4: Popelogan Granodiorite, 5: Magaguadavic Granite, 6: Dawson (McQuirks) Mtn, 7: Sorrel Ridge Granite, 8: Evandale Granodiorite, 9: Riviere Verte porphyry, 10: Nicholas Denys Granodiorite, 11: Falls Creek Granodiorite, 12: McKenzie Gulch porphyry, 13: Watson Brook Granodiorite.

$ZrTiO_4$ + SiO_2 A). A phase equilibrium investigation of the system "zircon + rutile + silicate melt/hydrothermal solution" at 1 GPa (Ferry and Watson, 2007) gives the amount of Ti in zircon as a function of temperature:

$$\log(\text{ppm Ti}) = 5.711 \pm 0.072 - 4800(\pm 86)/\text{T (K)}$$

This equation is more suitable for rocks formed under high pressure, such as granulite, which contains zircon, rutile, and quartz. Two points should be noted regarding the application of this equation. First, the absence of rutile in some granites indicates that a_{TiO_2} might be below unity when zircons formed. Second, even though granites are rich in SiO_2, a_{SiO_2} can be below unity during the initial stages of zircon crystallization (Schiller and Finger, 2019). Estimated temperatures for zircon crystallization in these I-type granitoids investigated were calculated using the Ti-in-zircon geothermometer by making corrections for reduced activities of TiO_2 and SiO_2 (Hanchar and Watson, 2003):

$$\log(\text{Ti ppm}) = 5.711 \pm 0.072 - 4800(\pm 86)/\text{T (K)} - \log\left(a_{SiO_2}\right) + \log\left(a_{TiO_2}\right)$$

Based on Hayden and Watson (2007), a_{TiO_2} is acceptable around 0.5, at which, the activity of silica for crystallization of zircon is approximately 1 (Ferry and Watson, 2007; Schiller and Finger, 2019). At first, Ferry and Watson (2007) proposed that the a_{TiO_2} ratio in rocks without rutile at magmatic temperatures is typically found to range between 0.6 and 0.9, seldom dipping below 0.5. According to Hayden and Watson (2007) and further investigations, and looking at all the references we mention above, it is more normal to use 0.5 for Ti activity. The trace element concentrations of

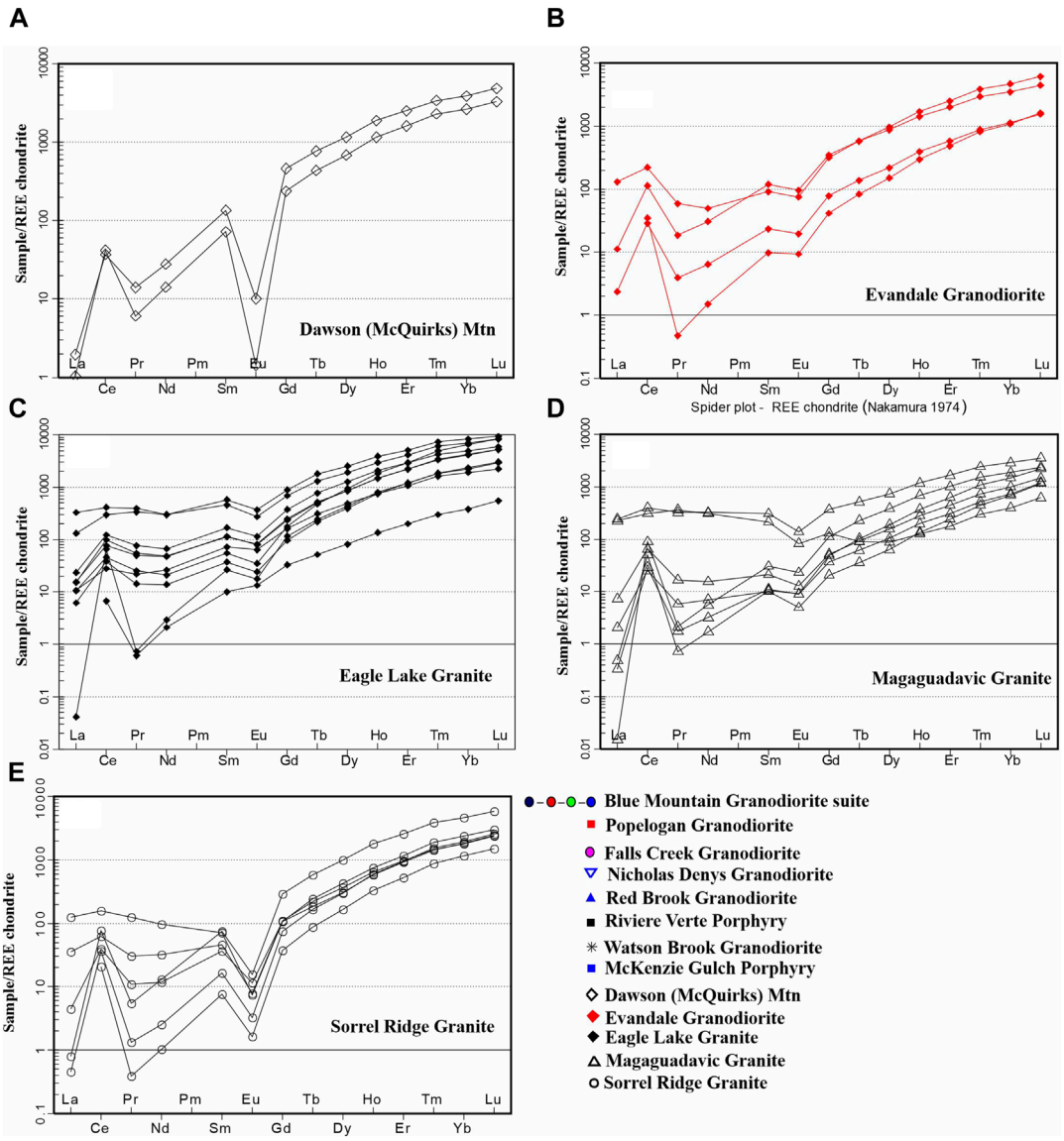

FIGURE 4
(Continued).

10.3389/feart.2024.1363029

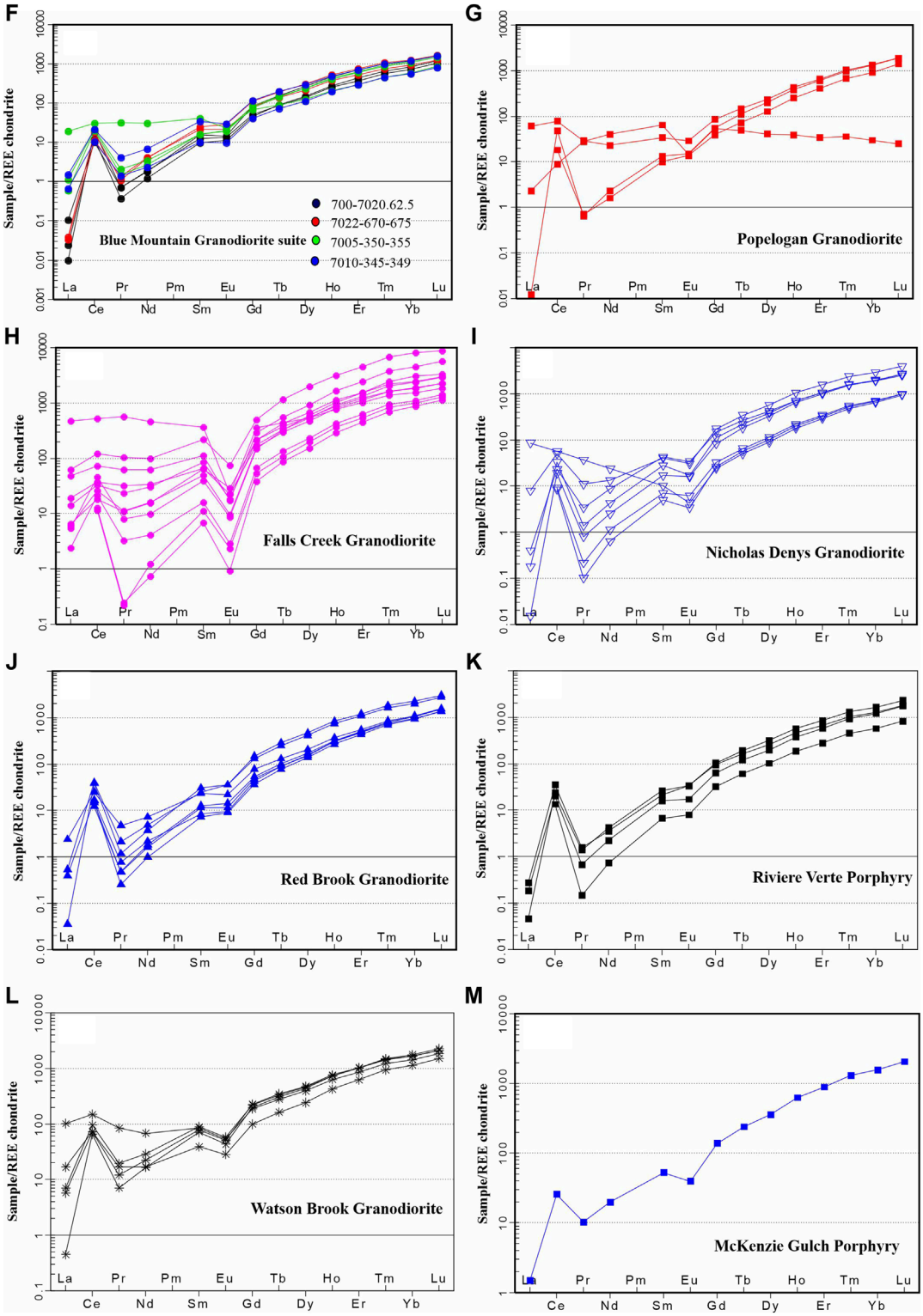

FIGURE 4
(Continued). Chondrite-normalized REE patterns of zircons from Devonian-aged oxidized I-type granodiorites of southern and northern parts of NB; Chondrite normalization values of Nakamura (1974). **(A)** Dawson (McQuirks) Mtn, **(B)** Evandale Granodiorite, **(C)** Eagle Lake Granite (ELG), **(D)** Magaguadavic Granite, **(E)** Sorrel Ridge Granite, **(F)** Blue Mountain Granodiorite Suite, **(G)** Popelogan granodiorite, **(H)** Falls Creek Granodiorite, **(I)** Nicholas Denys Granodiorite, **(J)** Red Brook Granodiorite, **(K)** Rivière Verte Porphyry, **(L)** Watson Brook Granodiorite, **(M)** McKenzie Gulch porphyry.

zircons investigated as well as crystallization temperatures of zircon calculated using the Ti-in-zircon geothermometer are presented in Table 2. Figure 5 shows a positive correlation between zircon Th/U and Ti-in-zircon temperature. The observed correlation, together with the positive relationship between Th/U (0.15–5.37) and Zr/Hf (24–60), suggests that higher temperature crystallization in less fractionated magmas is linked to increased zircon Th/U ratios. This is supported by work indicating that zircon in cooler and more fractionated melts contain more U, due to the typically more-incompatible character of U compared to Th (Kirkland et al., 2015). The calculated Ti-in-zircon temperature for these intrusions ranges from 737 (Rivière Verte Porphyry) to 899°C (Dawson Mtn); Note that unreasonable calculated temperatures are likely due to probable contamination during ablation and omitted from the calculated averages below. The average of these obtained temperatures is shown in Table 2.

Discrimination diagrams of Ti-in-zircon calculated temperature *versus* Hf (average: 9,136 ppm), U (average: 464 ppm), and Ce/Nd (average: 10.92) in zircon (Figure 6A, B, E, respectively) all show negative correlation. Samples from Watson Brook Granodiorite and Dawson Mountain do not exhibit a clear trend, as evident in all the diagrams. Rare earth element concentrations in zircons, and ratios (patterns) diverge systematically when compared to Hf and Ti. As can be seen in the chondrite normalized REE spider plots (Figure 4), zircons from the intrusions investigated all have positive Ce and negative Eu anomalies, and the magnitude of both increase as Hf concentration increases and calculated temperature decreases. The Eu/Eu*, Sm/Lu, and Ce/Nd are 0.01–0.73, 0.02–2.07, 1.3–41.07, respectively in these studied zircons (Figures 6C–E). In these zircons Ce/Ce* or Ce anomaly (it reflects variations in Ce^{4+}/Ce^{3+}) ranges from1.1 to 590. The Ce^{4+}/Ce^{3+} and Ce/Ce* are useful and important indicators of magmatic oxidation state (Loucks et al., 2020). The Ce/Ce* (Ce anomaly) is evaluated by interpolation between La and Pr ($Ce/Ce^* = Ce/\sqrt{[La^* Pr]}$), using chondrite normalization factors of Nakamura (1974), and Eu/Eu* (the europium anomaly) is calculated by the equation $Eu/\sqrt{[Sm^* Gd]}$. There are limitations regarding the calculation of the Ce anomaly, because the concentration of La and Pr in zircon are commonly at or near the detection limits of LA-ICP-MS using small laser crater diameters. According to Lu et al. (2016) and Ballard et al. (2002), use of the Ce/Nd ratio as a proxy for the Ce anomaly is appropriate (Figure 6E), because Ce and Nd occur in concentrations that are precisely measurable in zircon.

4.4 Magmatic oxygen fugacity

Zircon Ce and Eu anomalies are indicators of the oxidation state of magmas that form porphyry deposits (Loader et al., 2017). The Bulk geochemical composition of samples from the BMGS, ELG, Magaguadavic Granite, Nicholas Denys Granodiorite, Rivière Verte Porphyry, and Watson Brook Granodiorite, and the average trace element concentration of zircons are used to estimate the $\log fO_2$ of the melts during zircon crystallization following the method and Excel spreadsheet of Smythe and Brenan (2016). Based on Smythe and Brenan (2016), this method can be used for the rock group with high silica. The equation used is $\log fO_2$ (sample)–$\log fO_2$ (FMQ) = 3.998 (±0.124) $\log[Ce/\sqrt{(U^* Ti)^2}]$ + 2.28 (±0.10). In this method, due to the unavailability of geochemical data (major and minor elements) for all regions, the oxygen fugacity of some specific areas has been computed, although the geochemistry and trace elements concentration of all zircons is available. Also, the presented temperature is calculated Ti-in-zircon temperature (°C). $\log fO_2$ and ΔFMQ values for each area are as follows: Watson Brook Granodiorite ($\log fO_2$: 10.55, ΔFMQ: 2.47), Magaguadavic Granite ($\log fO_2$: 12.11, ΔFMQ: 3.87) which indicates high oxidation state in this intrusive suite, ELG ($\log fO_2$: 11.88, ΔFMQ: 1.74), Nicholas Denys Granodiorite ($\log fO_2$: 14.24, ΔFMQ: 1.15), BMGS ($\log fO_2$: 15.14, ΔFMQ: 0.77), and Rivière Verte Porphyry ($\log fO_2$: 15.57, ΔFMQ: 0.89) (Figure 7).

TABLE 2 Average calculated Ti-in-zircon temperature for oxidized I-type granitoids in NB.

Name of intrusion	Average calculated Ti-in-zircon temperature (°C)
Blue Mountain Granodiorite Suite (BMGS)	768°C
Eagle lake Granite (ELG)	883°C
Red Brook Granodiorite	772°C
Popelogan Granodiorite	767°C
Magaguadavic Granite	749°C
Dawson Mtn	899°C
Sorrel Ridge Granite	750°C
Evandale Granodiorite	761°C
Rivière Verte Porphyry	737°C
Nicholas Denys Granodiorite	749°C
Falls Creek Granodiorite	770°C
McKenzie Gulch Porphyry	813°C
Watson Brook Granodiorite	882°C

C° is calculated from Ti-in-zircon thermometer.

5 Discussion

5.1 Variation of trace elements in zircons

As we mentioned above, the studied zircons in this work are hosted by Devonian (Early, Middle, and Late) oxidized I-type granitoids with the porphyry Cu and Mo deposits and occurrences in NB, which these intrusions are situated in three Dunnage, Gander, and Avalon zones. As mentioned above, these studied intrusive rocks in NB do not show much difference in composition and are scattered between granodiorites and granites; throughout this research, the term "granitoids" is employed to describe these rock types. The intrusions investigated, along with previously published and newly acquired geochronologic constraints for oxidized porphyry-related intrusive rocks in the southern and central NB, include Sorrel

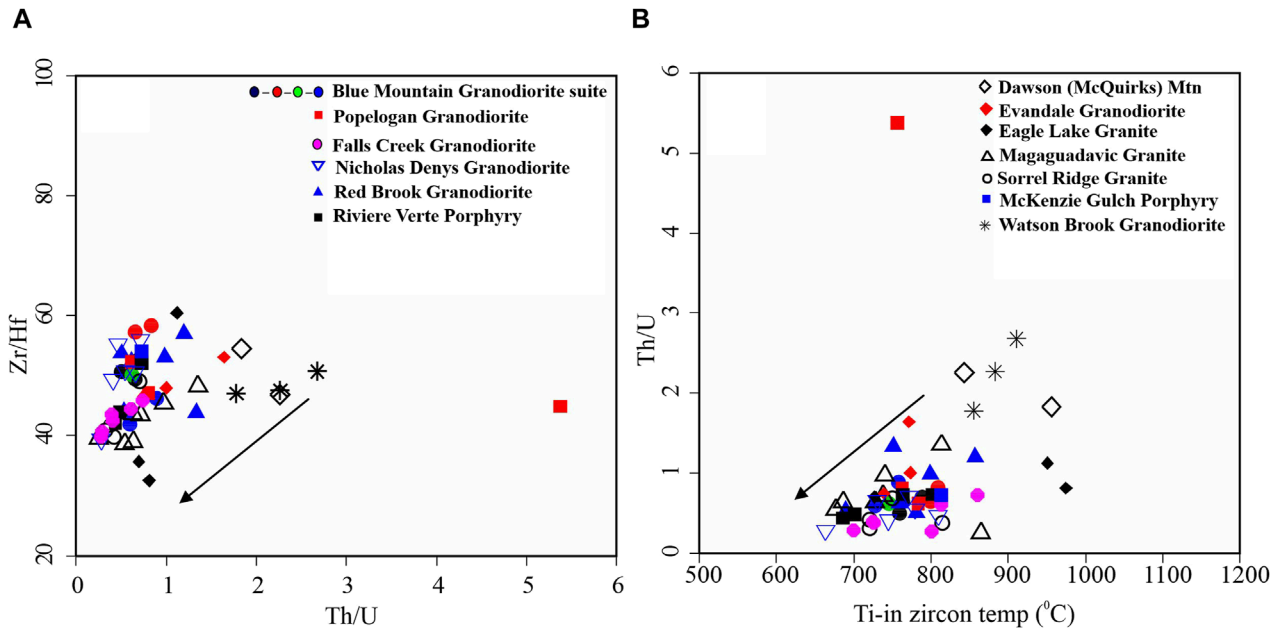

FIGURE 5
Trace element ratios in zircons examined during this study. **(A)** Zr/Hf *versus* Th/U and **(B)** Th/U *versus* Ti-in-zircon temperature in these studied I-type granitoids in NB.

Ridge Granite, Magaguadavic Granite, Eagle Lake Granite, Evandale Granodiorite, Dawson (McQuirks) Mtn, Red Brook Granodiorite, Falls Creek Granodiorite, and porphyry-related intrusions in northern NB contain BMGS, Nicholas Denys Granodiorite, Riviere Verte Porphyry, Watson Brook Granodiorite, McKenzie Gulch Porphyry, and Popelogan Granodiorite.

In this research, the utilization of zircon compositional analysis reveals a powerful tool for unraveling the complex evolution of each magma system. We utilized a straightforward textural classification, incorporating patchy zoning, homogeneous cores, oscillatory zoning, and unzoned zircon, to aid our discussion on the chemical composition and variations within zircons sourced from Devonian intrusions in NB, as discussed in the results section.

The trace element composition of zircon is influenced by the presence of co-crystallizing mineral phases such as amphibole, plagioclase, apatite, and titanite (Rezeau et al., 2019); this occurs because these minerals serve as sites for the incorporation of elements during magma crystallization. All REE has a +3-oxidation state; however, Ce and Eu have two other oxidation states in terrestrial magmas. Specifically, the oxidized forms (Ce^{4+} 0.97 Å and Eu^{3+} 1.066 Å) are more favorably incorporated into the zircon lattice, whereas the reduced forms (Ce^{3+} 1.143 Å) and Eu^{2+} 1.25 Å) are generally excluded, because of the greater charge to radius ratios. Therefore, the magnitude of the positive Ce anomaly and negative Eu anomaly in zircons from intrusions investigated in this study (see Figure 4) all indicate a relatively high magmatic oxidation state. According to Massawe and Lentz, (2020), major element geochemical data for whole rocks from certain intrusions exhibit adakitic characteristics such as $SiO_2 \geq 56$ wt%, $Al_2O_3 \geq 15$ wt%, and MgO <3 wt% (rarely >6 wt%). Likewise, concentrations of selected trace elements Y and heavy rare earth elements (HREE) are low (e.g., Y ≤ 18 ppm and Yb = 1.9 ppm), and Sr concentrations are high (>400 ppm), and also indicate an adakitic magma. Plagioclase fractionation before or during the saturation of zircon preferentially removes Eu from the melt resulting in a negative Eu anomaly in zircon (Smythe and Brenan, 2015). Shu et al. (2019) described the factors that affect the measurement of trace elements in zircon and consequently its usefulness as a proxy for oxidation state. Specifically, it is important the zircon cannot be influenced by other magmatic processes. This may not always be the case as prior or concurrent crystallization of other REE-bearing minerals (e.g., plagioclase, titanite, and monazite) could change the resultant REE patterns and the calculated Eu anomaly. For example, crystallization of plagioclase before or during the saturation of zircon will result in negative Eu anomaly in zircon (Smythe and Brenan, 2015), whereas crystallization of titanite will generate a positive Eu anomaly (Loader et al., 2017; Shu et al., 2019). It should be noted that the Ce anomaly is a more robust proxy for magma oxidation state than the Eu anomaly (Shu et al., 2019). This assertion is supported by the stronger correlation observed in the Ce anomalies of oxidized I-type granitoids of NB ($Ce/Ce^* = 1.1–570$; Ce/Nd = 1.3–41.07), surpassing the correlation between the Eu anomaly and deposit size. Loucks et al. (2020) asserted that zircon/melt partition coefficients of Ce and U vary inversely with fO_2 in silicate melts. Davidson et al. (2007) and Wang et al. (2019) indicated that preferential sequestration of middle REE (e.g., Dy) over heavy- and light- REE can only readily be explained by the involvement of amphibole, which preferentially incorporates middle REE relative to the light and heavy REE. Therefore, amphibole fractionation in hydrous melts can account for the reduction of Dy/Yb (<0.4) ratio in the melts and in the crystallized zircon.

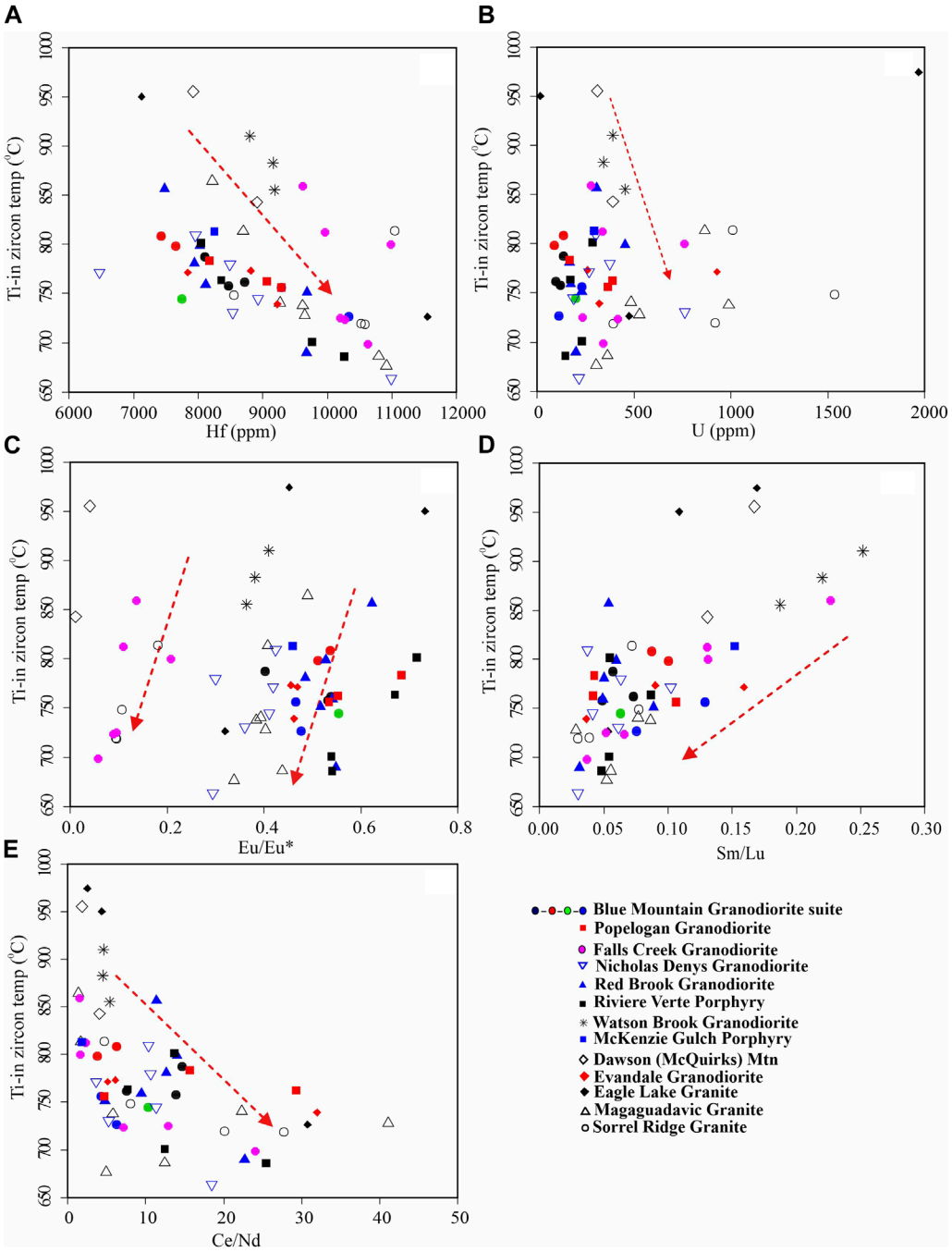

FIGURE 6
Trace element chemistry of zircons examined during this study, and Ti-in-zircon Temperature *versus* **(A)** U ppm and **(B)** Hf ppm, **(C)** Eu/Eu* *versus* T_{TiZr}, **(D)** Sm/Lu *versus* T_{TiZr}, **(E)** Ce/Nd *versus* T_{TiZr}.

Zirconium and Hf are nearly identical geochemically and the Zr/Hf ratio in the zircons examined in this study ranges from 24 to 60. Zircon is the primary reservoir for both Zr and Hf but preferentially incorporates Zr. Therefore, the crystallization of zircon controls the Zr/Hf of the melt which decreases with increasing fractionation of zircon (cf. Claiborne et al., 2006). Low Zr/Hf reflects more extensive magmatic fractionation, and high Hf (low Zr/Hf) in zircon indicates growth from a highly fractionated melt. According to Davidson et al. (2000) and Aranovich and Bortnikov (2018), Zr and Hf may be fractionated from each other to some extent by minerals, such as amphibole, clinopyroxene, titanite, garnet, and ilmenite. Thus, the bulk-rock Zr/Hf might differ from the melt from which the zircon started to crystallize (Aranovich and Bortnikov, 2018). Claiborne et al. (2006) noted that the reduction in Zr, Hf, and Zr/Hf indicates crystallization and removal of zircon. Based on Claiborne et al. (2006) and Miller et al.

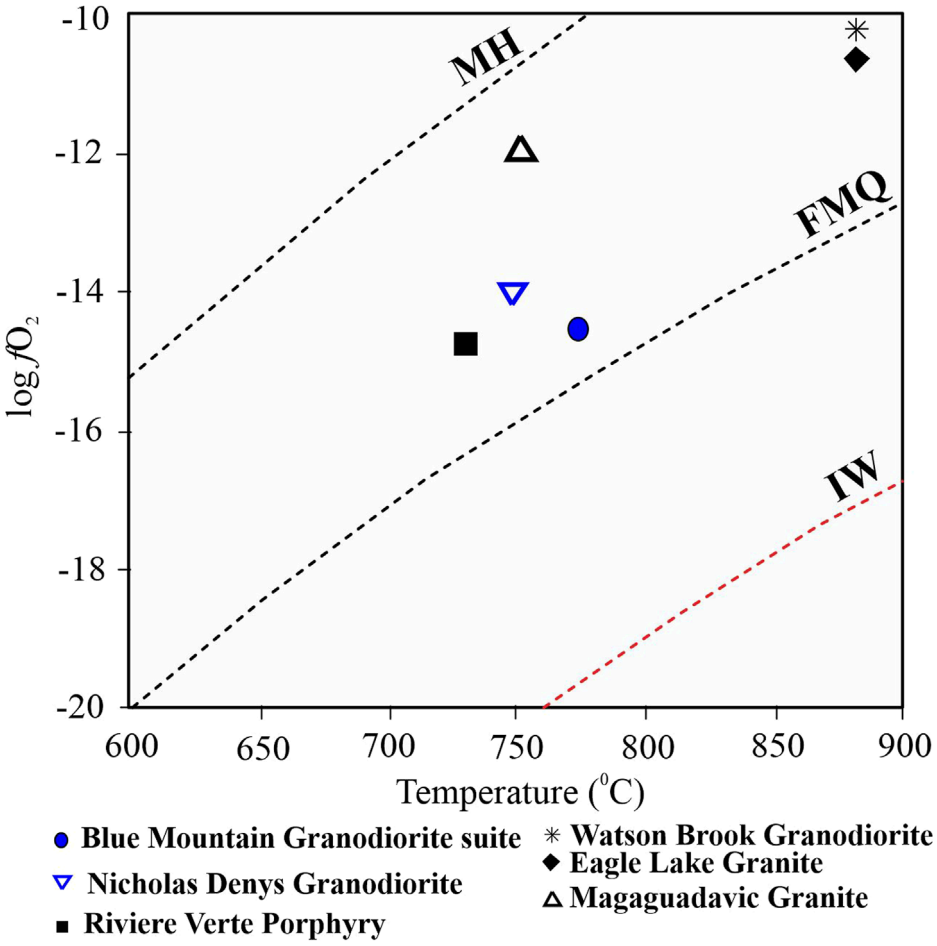

FIGURE 7
Values of logfO_2 vs. T ºC in the NB granodiorite samples. The logfO_2 is calculated based on the method in Smythe and Brenan (2016). The equation used is logfO_2 (sample)−log fO_2 (FMQ) = 3.99 (±0.12) log[Ce/$\sqrt{}$(U* Ti)^2] + 2.28 (±0.10). The dashed black lines match up with variation in fO_2 with T along IW (iron-wüstite), FMQ (fayalite-magnetite-quartz), and MH (magnetite-hematite) buffers.

(2005), low whole-rock Zr/Hf indicates effective extraction of evolved melt after extensive crystallization of zircon. The average of Zr/Hf in the available rock data of some of the intrusions investigated is BMGS = 39, ELG = 33, Magaguadavic Granite =34, Nicholas Denys Granodiorite =38, Rivière Verte Porphyry= 38, and Watson Brook Granodiorite =40. In Azadbakht et al. (2019) divided New Brunswick granites into three categories: NB-1, NB-2, and NB-3 based on geochemical variations. Some of the intrusions investigated in this study were also investigated by Azadbakht et al. (2019). Specifically, the Nicholas Denys Granodiorite and Magaguadavic Granite belong to the NB-1 group, whereas the Sorrel Ridge Granite belongs to the NB-2. NB-1 is the product of partial melting of lower crust, and NB-2 granites are the product of different degrees of assimilation-fractional crystallization (AFC) and where mineralization is present in some porphyries secondary hydrothermal alteration occurs to a variable extent (Azadbakht et al., 2019).

The Hf/Y and Th/U of zircons investigated in this study are consistent with an evolving magmatic system from early amphibole-dominated fractionation to amphibole ± apatite ± titanite (Figure 8). Lee et al. (2021) and Gagnevin et al. (2010) postulated that as a melt evolves to more silicic compositions, the concentrations of U, Th, and Y generally increase, and Th/U of co-crystallizing zircon typically decreases. It should be noted that amphibole is the dominant crystallizing ferromagnesian phase in these mafic to intermediate magmas, which is indicative of higher hydrous component; also, Y and HREE are removed from the melt as they readily fractionate into amphibole thereby increasing the Hf/Y (*cf.* Lee et al., 2021). In these studied zircon Hf/Y and Th/U are between 0.03–34 and 0.two to three, respectively (Figure 8). The elevated Yb/Gd$_N$ and low Hf/Y are consistent with the more felsic intrusions, such as ELG (Yb/Gd$_N$= 3.4). The Hf concentration of zircon is a gauge of magmatic differentiation with the Hf concentrations in zircon increasing during differentiation from mafic to felsic melts (Rezeau et al., 2019), and the Hf concentration is inversely related to Ti, which reflects progressive cooling during differentiation. The Eu/Eu* of these zircons is >0.3, and as described above, is characteristic of ore-forming arc magmas (Lee et al., 2021). Based on the above results, most of the oxygen fugacity (log fO_2) of the magmas were higher than FMQ+2 (FMQ is the fayalite-magnetite-quartz oxygen fugacity buffer). High fO_2 is typical in fertile porphyry systems, whereas an fO_2 < FMQ+2 is

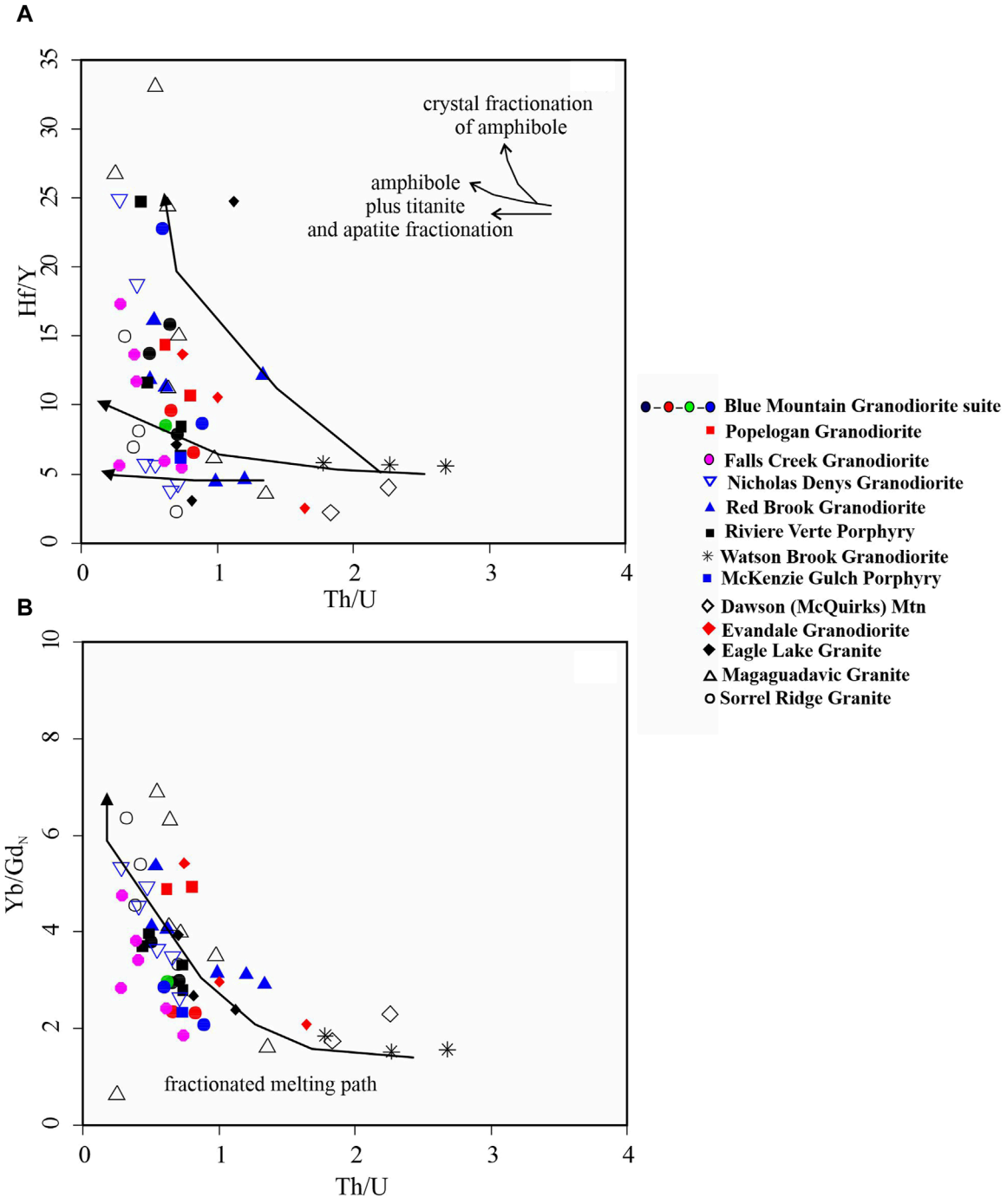

FIGURE 8
Trace-element compositional systematics diagrams for zircons in the NB Devonian oxidized I-type granodiorites; **(A)** Th/U *versus* Hf/Y, **(B)** Th/U *versus* $(Yb/Gd)_N$. (Fractionated melting paths and mixing lines after Lee et al., 2021).

typical of infertile systems, and ore-forming intrusions typically crystallized from highly oxidized and hydrous melts with oxygen fugacity more than FMQ+2 and water contents up to 12 wt% (Lu et al., 2016). The presence of magnetite and ilmenite in most of the 13 intrusions examined partially constrains the oxygen fugacity in these porphyry systems to values close to the FMQ oxygen buffer.

5.2 Fertility and infertility of intrusions

Trace-element concentration in zircon can track the hydration and oxidation states of the magma in which they formed and consequently identify those systems with the greatest potential to host porphyry Cu±Mo±Au systems (Ballard et al., 2002; Lee et al., 2021). According to Richards (2003), porphyry copper deposits

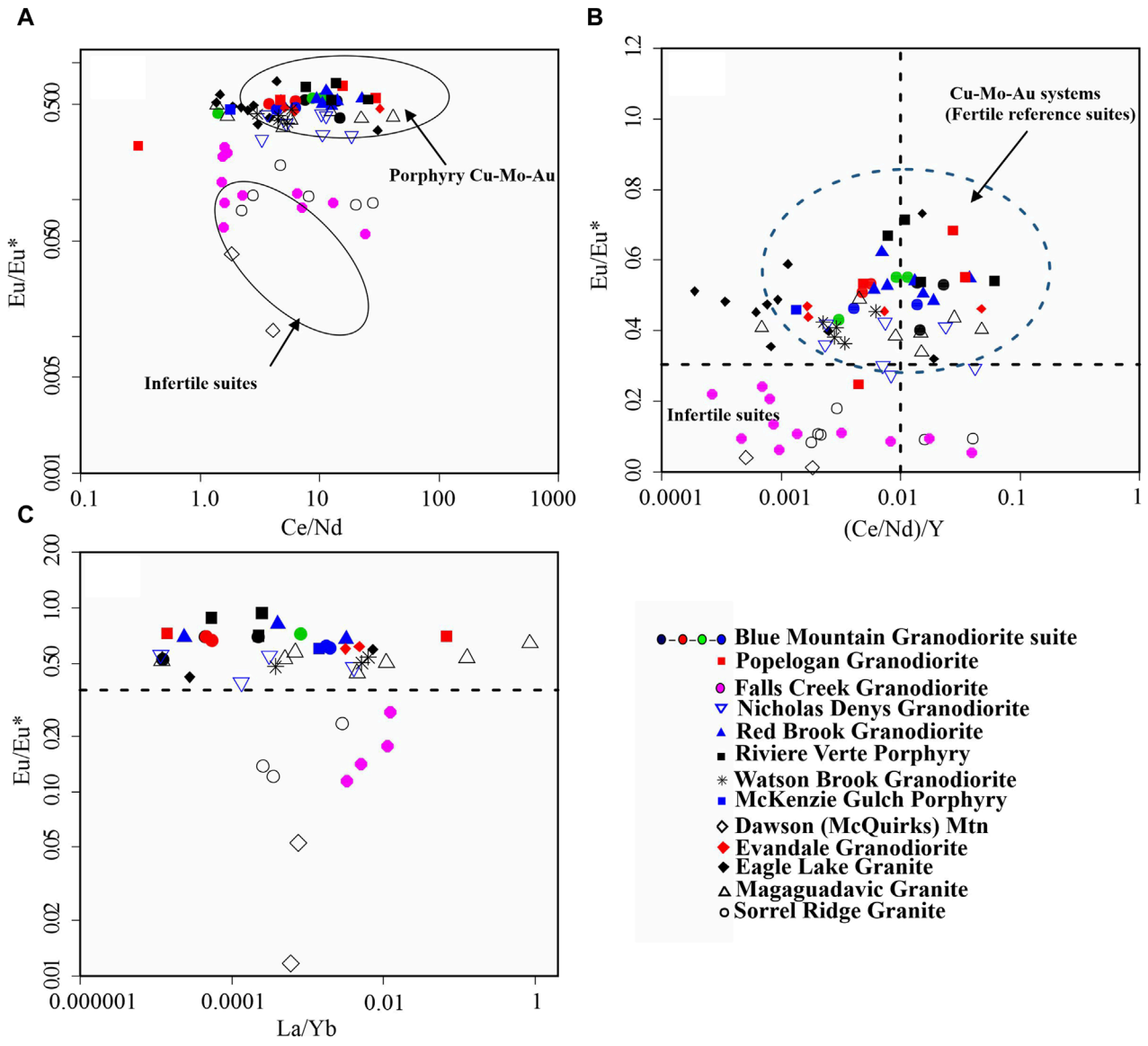

FIGURE 9
Zircons' trace-element-based discrimination diagrams showing fertility *versus* infertility of oxidized I-type granite in NB. **(A)** Zircon Eu/Eu* *versus* Ce/Nd, **(B)** Zircon Eu/Eu* *versus* (Ce/Nd)/Y. The fields of fertile Cu-Mo-Au systems and infertile suites in Supplementary Figure SA, B are from Lu et al. (2016). **(C)** Zircon Eu/Eu* *versus* La/Yb.

form from fluids exsolved from moderately oxidized, silica-rich melts with high S, Cl, and water content. All of the intrusions investigated are Early to Late Devonian, and were emplaced in late- to post-tectonic setting relative to the Acadian orogeny, and all are oxidized I-type granitoids with adakitic features and have spatially and temporally associated Cu-Mo (Au) mineralization. The relationship between high Sr/Y and La/Yb magmas (adakites) and their role as progenitors to porphyry Cu-Au-Mo mineralization is one of the most interesting discussions of the day (Whalen and Hildebrand, 2019). Porphyry and skarn Cu and Mo deposits are usually produced by oxidized magmas (Blevin and Chappell, 1992). Based on Shu et al. (2019), oxidized magmas can extract more Cu (and Mo) from source rocks during melting than reduced magmas, and magmas with high oxygen fugacities can absorb significant amounts of sulfur during ascent, both of which are necessary for metallic sulfide formation. Here, trace-element datasets are used for recognizing the fertility and infertility of these oxidized I-type granite (Yousefi et al., 2023a). Differentiating fertile and infertile intrusions can be accomplished using zircon trace element ratios such as Eu/Eu*, Ce/Nd, (Ce/Nd)/Y, and (Eu/Eu*)/Y. Most of the zircons from fertile systems have high zircon Eu/Eu* (>0.3) and (Ce/Nd)/Y between 0.001–1.0, whereas those from Cu-infertile systems, i.e., Falls Creek Granodiorite and Sorrel Ridge Granite, have (Eu/Eu* <0.3; Figures 9A, B), that have low grade Mo-only with some Au potential but no known Cu mineralization.

The Eu/Eu^* of zircons from the intrusions such as Falls Creek Granodiorite, Dawson (McQuirks) Mtn, and Sorrel Ridge Granite are significantly lower than those of the other intrusions in the dataset. Samples from the Falls Creek Granodiorite and Sorrell Ridge granites plot in the infertile suite fields on Figures 9A, B, with decreasing Eu/Eu^* with increasing Ce/Nd, relative to fertile intrusions that commonly have constant Eu/Eu^* with increasing Ce/Nd (0.3–41.07). It is worth mentioning that while the zircon samples from Falls Creek Granodiorite and Sorrell Ridge Granite in Figure 9A do not exhibit a distinct trend, they align more with the infertile suite. The constant or high zircon Eu/Eu^* in fertile intrusions reflects high magmatic water content and/or high oxidation state in the host magma (Dilles et al., 2015). Figure 9C shows obvious variation in La/Yb, but lower La/Yb is more important in fertile porphyry system. As depicted in Figure 6C, the Eu/Eu∗ value for NB's zircon ranges from ≥0.01 to 0.73, suggesting a significant potential for porphyry Cu formation in NB. The high Ce^{4+}/Ce^{3+} (1.1–590) and negative Eu/Eu^* >0.4 in NB studied zircon are characteristic of ore-forming arc magmas, such as those Chuquicamata-El Abra porphyry copper belt of northern Chile that have zircon with Ce^{4+}/Ce^{3+}>300 and Eu/Eu^* >0.4 (Ballard et al., 2002). Higher Ce/Ce^* (1.1–590) implies more oxidizing (metallogenically favorable) conditions (diminished Eu anomaly); lower Eu contents reflects reducing conditions, where Eu^{2+} does not readily substitute into the zircon lattice, whereas in highly oxidized systems the concentration of Eu^{2+} is low. Lu et al. (2016) reinforced the analysis of key ratios, such as Eu/Eu^* >0.3 in zircon, as a strong indicator of ore-forming intrusions, such as those associated with Batu Hijau and Tampakan, El Salvador, Chile, and Sar Cheshmeh porphyry Cu-Au deposits.

6 Conclusion

Combining the zircon fertility indicators described above, it is possible to discriminate less prospective A-, S, and I-type granitoids from oxidized I-type granitoids that are more prospective for Cu-Mo-Au mineralization. Zircon from the granitoids sampled in this study have a large range of trace- and minor-element (Hf, HREE, Th, U) compositions. The positive correlation between Th/U (0.15–5.37) and Zr/Hf (24–60) indicates that higher temperature crystallization of less fractionated magmas is reflected by high Th/U in zircon. Ce/Ce^* (Ce anomaly) values are in the range of 1.1–590; with higher Ce/Ce^* reflecting more metallogenically favourable oxidizing conditions. Zircon Zr/Hf and Eu/Eu^* (≥0.4) and $(Eu/Eu^*)/Y$ values, as well as zircon (Ce/Nd)/Y (0.001–1.0) are some of the best fertility indicators. The geochemical features of these I-type intrusions in NB, such as low amount of HREE and Y, are similar to adakitic rocks. According to Whalen and Hildebrand (2019) and ratios of trace elements, the genesis of these rocks has been linked to slab failure in the late to post Acadian orogeny. The calculated Ti-in-zircon saturation temperature for the I-type oxidized granitoids ranges from 737 to 899°C (Rivière Verte Porphyry to Dawson Mtn). The calculated $\log fO_2$ values for zircons from the investigated granitoids indicate crystallization from highly oxidized magmas, with the highest being the Magaguadavic Granite with $\log fO_2$ values (average = −12.11) ΔFMQ average value = 3.87.

The results from LA-ICP-MS analysis on zircons from oxidized I-type granitoids show that with the exception of the Falls Creek Granodiorite, Sorrel Ridge Granite, and Dawson Mtn all of the granitoids examined, plot in the field of with potential Cu±Mo±Au mineralization. High Eu/Eu^* in zircon (i.e. ≥ 0.4) indicates relatively oxidized conditions, and fingerprints ore-forming porphyry Cu-Mo associated with these oxidized I-type granitoids, and is consistent with magmas originating from mantle or juvenile oceanic or crustal source with a small component of older crust. As confirmed in this study, zircon composition has considerable potential to be used as a pathfinder for porphyry Cu±Mo±Au systems.

Data availability statement

The datasets presented in this study can be found in online repositories. The names of the repository/repositories and accession number(s) can be found in the article/Supplementary Material.

Author contributions

FY: Writing–original draft. DL: Supervision, Writing–review and editing. CM: Supervision, Writing–review and editing. JW: Writing–review and editing. KT: Writing–review and editing.

Funding

The author(s) declare that financial support was received for the research, authorship, and/or publication of this article. Funding for this project was provided by NB Geological Survey (NB Department of Natural Resources and Energy Development) and University of New Brunswick to DL.

Acknowledgments

We thank Brandon Boucher (UNB) for help with LA-ICP-MS analysis of zircons. Dr. Doug Hall and Steve Cogswell helped with the SEM imaging in the UNB MMF unit. The authors gratefully acknowledge the reviewers and the editors for their constructive comments to improve this article.

Conflict of interest

The authors declare that the research was conducted in the absence of any commercial or financial relationships that could be construed as a potential conflict of interest.

The author(s) declared that they were an editorial board member of Frontiers, at the time of submission. This had no impact on the peer review process and the final decision.

Publisher's note

All claims expressed in this article are solely those of the authors and do not necessarily represent those of their affiliated organizations, or those of the publisher, the editors and the reviewers. Any product that may be evaluated in this article, or claim that may be made by its manufacturer, is not guaranteed or endorsed by the publisher.

Supplementary material

The Supplementary Material for this article can be found online at: https://www.frontiersin.org/articles/10.3389/feart.2024.1363029/full#supplementary-material

References

Aranovich, L. Y., and Bortnikov, N. S. (2018). New Zr–Hf geothermometer for magmatic zircons. *J. Petrol.* 26, 115–120. doi:10.1134/S0869591118020029

Azadbakht, Z., Lentz, D. R., and McFarlane, C. R. (2018). Apatite chemical compositions from Acadian-related granitoids of New Brunswick, Canada: implications for petrogenesis and metallogenesis. *Minerals* 8 (12), 598. doi:10.3390/min8120598

Azadbakht, Z., McFarlane, C. R. M., and Lentz, D. R. (2016). Precise U-Pb ages for the cogenetic alkaline Mount LaTour and peraluminous Mount Elizabeth granites of the South Nepisiguit River plutonic suite, northeastern New Brunswick, Canada. *Atl. Geol.* 52, 188–211. doi:10.4138/atlgeol.2016.009

Azadbakht, Z., Rogers, N., Lentz, D. R., and McFarlane, C. R. M. (2019). "Petrogenesis and associated mineralization of Acadian related granitoids in New Brunswick," in *Targeted Geoscience Initiative: 2018 Report of Activities*. Editor N. Rogers (Geological Survey of Canada), 8549, 243–278. Open File. doi:10.4095/313658

Bacon, C. R. (1989). Crystallization of accessory phases in magmas by local saturation adjacent to phenocrysts. *Geochim. Cosmochim. Acta.* 53 (5), 1055–1066. doi:10.1016/0016-7037(89)90210-X

Ballard, J. R., Palin, J. M., and Campbell, I. H. (2002). Relative oxidation states of magmas inferred from Ce (IV)/Ce (III) in zircon: application to porphyry copper deposits of northern Chile. *Contrib. Mineral. Petrol.* 144, 347–364. doi:10.1007/s00410-002-0402-5

Blevin, P. L., and Chappell, B. W. (1992). The role of magma sources, oxidation states and fractionation in determining the granite metallogeny of eastern Australia. *Earth Environ. Sci. Trans. R. Soc. Edinb.* 83 (1-2), 305–316. doi:10.1017/S0263593300007987

Burnham, C. W. (1979). "Magmas and hydrothermal fluids," in *Geochemistry of Hydrothermal Ore Deposits*. H.L. Barnes. 2nd edition (New York: John Wiley and Sons).

Claiborne, L. L., Miller, C. F., Walker, B. A., Wooden, J. L., Mazdab, F. K., and Bea, F. (2006). Tracking magmatic processes through Zr/Hf ratios in rocks and Hf and Ti zoning in zircons: an example from the Spirit Mountain batholith, Nevada. *Mineral. Mag.* 70 (5), 517–543. doi:10.1180/0026461067050348

Cooke, D. R., Agnew, P., Hollings, P., Baker, M., Chang, Z., Wilkinson, J. J., et al. (2020). Recent advances in the application of mineral chemistry to exploration for porphyry copper–gold–molybdenum deposits: detecting the geochemical fingerprints and footprints of hypogene mineralization and alteration. *Geochem. Explor. Environ. Anal.* 20 (2), 176–188. doi:10.1144/geochem2019-039

Courtney-Davies, L., Ciobanu, C. L., Verdugo-Ihl, M. R., Slattery, A., Cook, N. J., Dmitrijeva, M., et al. (2019). Zircon at the nanoscale records metasomatic processes leading to large magmatic–hydrothermal ore systems. *Minerals* 9 (6), 364. doi:10.3390/min9060364

Davidson, J., Turner, S., Handley, H., Macpherson, C., and Dosseto, A. (2007). Amphibole "sponge" in arc crust? *Geology* 35 (9), 787–790. doi:10.1130/g23637a.1

Davidson, J. P., Turner, S. P., and Macpherson, C. G. (2008). Water storage and amphibole control in arc magma differentiation. *Geochim. Cosmochim. Acta.* 72 (12), A201.

Dilles, J. H., Kent, A. J. R., Wooden, J. L., Tosdal, R. M., Koleszar, A., Lee, R. G., et al. (2015). Zircon compositional evidence for sulfur-degassing from ore-forming arc magmas. *Econ. Geol.* 110, 241–251. doi:10.2113/econgeo.110.1.241

Ferry, J. M., and Watson, E. B. (2007). New thermodynamic models and revised calibrations for the Ti-in-zircon and Zr-in-rutile thermometers. *Contrib. Mineral. Petrol* 154 (4), 429–437. doi:10.1007/s00410-007-0201-0

Fowler, A., Prokoph, A., Stern, R., and Dupuis, C. (2002). Organization of oscillatory zoning in zircon: analysis, scaling, geochemistry, and model of a zircon from Kipawa, Quebec, Canada. *Geochim. Cosmochim. Acta* 66 (2), 311–328. doi:10.1016/S0016-7037(01)00774-8

Frost, B. R., Barnes, C. G., Collins, W. J., Arculus, R. J., Ellis, D. J., and Frost, C. D. (2001). A geochemical classification for granitic rocks. *J. Petrol.* 42 (11), 2033–2048. doi:10.1093/petrology/42.11.2033

Fu, B., Page, F. Z., Cavosie, A. J., Fournelle, J., Kita, N. T., Lackey, J. S., et al. (2008). Ti-in-zircon thermometry: applications and limitations. *Contrib. Mineral. Petrol.* 156 (2), 197–215. doi:10.1007/s00410-008-0281-5

Fyffe, L. R., Johnson, S. C., and van Staal, C. R. (2011). A review of proterozoic to early paleozoic lithotectonic terranes in new Brunswick, Canada and their tectonic evolution during Penobscot, Taconic, Salinic and Acadian orogenesis. *Atl. Geol.* 47, 211–248. doi:10.4138/atlgeol.2011.010

Fyffe, L. R., Thorne, K. G., Dunning, G. R., and Martin, D. A. (2008). "U–Pb geochronology of the Sisson Brook granite porphyry, York County, west-central New Brunswick," in *Geological investigations in New Brunswick for 2007*. Editor G. L. Martin, 35–54. New Brunswick Department of Natural Resources; Minerals, Policy and Planning Division, *Mineral Resource Report* 2008–1.

Gagnevin, D., Daly, J. S., and Kronz, A. (2010). Zircon texture and chemical composition as a guide to magmatic processes and mixing in a granitic environment and coeval volcanic system. *Contrib. Mineral. Petrol.* 159, 579–596. doi:10.1007/s00410-009-0443-0

Halden, N. M., Hawthorne, F. C., Campbell, J. L., Teesdale, W. J., Maxwell, J. A., and Higuchi, D. (1993). Chemical characterization of oscillatory zoning and overgrowths in zircon using 3 MeV mu-PIXE. *Can. Mineral.* 31 (3), 637–647.

Hanchar, J. M., and Watson, E. B. (2003). Zircon saturation thermometry. *Rev. Mineral. Geochem.* 53 (1), 89–112. doi:10.2113/0530089

Hayden, L. A., and Watson, E. B. (2007). Rutile saturation in hydrous siliceous melts and its bearing on Ti-thermometry of quartz and zircon. *Earth Planet Sci. Lett.* 258, 561–568. doi:10.1016/j.epsl.2007.04.020

Hibbard, J. P., Van Staal, C. R., Rankin, D. W., and Williams, H. (2006). *Lithotectonic map of the Appalachian orogen, Canada-United States of America*. Geological Survey of Canada: Natural Resources Canada. map 2096A, Scale 1:1 500000.

Hollister, V. F., Potter, R. R., and Barker, A. L. (1974). Porphyry-type deposits of the Appalachian orogen. *Econ. Geol.* 69 (5), 618–630. doi:10.2113/gsecongeo.69.5.618

John, D. A., Ayuso, R. A., Barton, M. D., Blakely, R. J., Bodnar, R. J., Dilles, J. H., et al. (2010). *Porphyry copper deposit model, chap. B of Mineral Deposit Models for Resource Assessment*. U.S. Geological Survey Scientific Investigations Report 2010–5070–B, 169.

Kellett, D. A., Piette-Lauzière, N., Mohammadi, N., Bickerton, L., Kontak, D., Rogers, N., et al. (2021). Spatio-temporal distribution of Devonian post-accretionary granitoids in the Canadian Appalachians: implications for tectonic controls on intrusion related mineralization. *Geol. Surv. Can. Target. Geoscience Initiative (TGI)* 5, 7–23. doi:10.4095/327955

Kemp, A. I., Hawkesworth, C. J., Foster, G. L., Paterson, B. A., Woodhead, J. D., Hergt, J. M., et al. (2007). Magmatic and crustal differentiation history of granitic rocks from Hf-O isotopes in zircon. *Science* 315, 980–983. doi:10.1126/science.1136154

Kirkland, C. L., Smithies, R. H., Taylor, R. J. M., Evans, N., and McDonald, B. (2015). Zircon Th/U ratios in magmatic environs. *Lithos* 212, 397–414. doi:10.1016/j.lithos.2014.11.021

Lee, R. G., Byrne, K., D'Angelo, M., Hart, C. J., Hollings, P., Gleeson, S. A., et al. (2021). Using zircon trace element composition to assess porphyry copper potential of the Guichon Creek batholith and Highland Valley Copper deposit, south-central British Columbia. *Min. Depos.* 56, 215–238. doi:10.1007/s00126-020-00961-1

Loader, M. A., Wilkinson, J. J., and Armstrong, R. N. (2017). The effect of titanite crystallisation on Eu and Ce anomalies in zircon and its implications for the assessment of porphyry Cu deposit fertility. *Earth Planet Sci. Lett.* 472, 107–119. doi:10.1016/j.epsl.2017.05.010

Loucks, R. R., Fiorentini, M. L., and Henríquez, G. J. (2020). New magmatic oxybarometer using trace elements in zircon. *J. Petrol.* 61 (3), egaa034. doi:10.1093/petrology/egaa034

Lu, Y. J., Loucks, R. R., Fiorentini, M., McCuaig, T. C., Evans, N. J., Yang, Z. M., et al. (2016). Zircon compositions as a pathfinder for porphyry Cu±Mo±Au deposits

Society of Economic Geologists Special. *Tect. Metallogeny Tethyan orogenic Belt* 19, 1–57. doi:10.5382/SP.19.13

Luo, Y., and Ayers, J. C. (2009). Experimental measurements of zircon/melt trace-element partition coefficients. *Geochim. Cosmochim. Acta.* 73 (12), 3656–3679. doi:10.1016/j.gca.2009.03.027

Massawe, R. J., and Lentz, D. R. (2020). Petrochemistry and U–Pb (zircon) age of porphyry dykes at the McKenzie Gulch porphyry–skarn Cu–Ag–Au deposit, north-central New Brunswick, Canada: implications for emplacement age, tectonic setting, and mineralization potential. *Can. J. Earth Sci.* 57 (4), 427–452. doi:10.1139/cjes-2018-0313

Miller, C. F., Lowery, L. E., and Bea, F. (2005). Zircon and Zr/Hf ratios: assessing magmatic fractionation in the crust. *Geochim. Cosmochim. Acta.* 69, A10.

Mohammadi, N., Fyffe, L., McFarlane, C. R., Thorne, K. G., Lentz, D. R., Charnley, B., et al. (2017). Geological relationships and laser ablation ICP-MS U-Pb geochronology of the Saint George Batholith, southwestern New Brunswick, Canada: implications for its tectonomagmatic evolution. *Atl. Geol.* 53, 207–240. doi:10.4138/atlgeol.2017.008

Nakamura, N. (1974) Determination of REE, Ba, Fe, Mg, Na and K in Carbonaceous and Ordinary Chondrites. *Geochimica et Cosmochimica Acta*, 38, 757–775. doi:10.1016/0016-7037(74)90149-5

Rezeau, H., Moritz, R., Wotzlaw, J. F., Hovakimyan, S., and Tayan, R. (2019). Zircon petrochronology of the Meghri-Ordubad pluton, Lesser Caucasus: fingerprinting igneous processes and implications for the exploration of porphyry Cu-Mo deposits. *Econ. Geol.* 114 (7), 1365–1388. doi:10.5382/econgeo.4671

Richards, J. P. (2003). Tectono-magmatic precursors for porphyry Cu-(Mo-Au) deposit formation. *Econ. Geol.* 98, 1515–1533. doi:10.2113/gsecongeo.98.8.1515

Ruitenberg, A. A., and Fyffe, L. R. (1982). Mineral deposits associated with granitoid intrusions and related subvolcanic stocks in New Brunswick and their relationship to Appalachian tectonic evolution. *Can. Inst. Min. Metallurgy. Bull.* 75 (842), 83–97.

Ruitenberg, A. A., McCutcheon, S. R., Venugopal, D. V., and Pierce, G. A. (1977). Mineralization related to post-Acadian tectonism in southern New Brunswick. *Geosci. Can.* 4 (1). Available at: https://journals.lib.unb.ca/index.php/GC/article/view/2981.

Schiller, D., and Finger, F. (2019). Application of Ti-in-zircon thermometry to granite studies: problems and possible solutions. *Contrib. Mineral. Petrol.* 174, 51–16. doi:10.1007/s00410-019-1585-3

Shu, Q., Chang, Z., Lai, Y., Hu, X., Wu, H., Zhang, Y., et al. (2019). Zircon trace elements and magma fertility: insights from porphyry (-skarn) Mo deposits in NE China. *Min. Depos.* 54, 645–656. doi:10.1007/s00126-019-00867-7

Sillitoe, R. H. (2010). Porphyry copper systems. *Econ. Geol.* 105, 3–41. doi:10.2113/gsecongeo.105.1.3

Sinclair, W. D. (2007). "Porphyry deposits," in *Mineral Deposits of Canada: a synthesis of major Deposit-types, district metallogeny, the evolution of geological provinces, and exploration methods*. Editor W. D. Goodfellow (Geological Association of Canada, Mineral Deposits Division), 5, 223–243.

Smythe, D. J., and Brenan, J. M. (2015). Cerium oxidation state in silicate melts: combined fO_2, temperature and compositional effects. *Geochim. Cosmochim. Acta.* 170, 173–187. doi:10.1016/j.gca.2015.07.016

Smythe, D. J., and Brenan, J. M. (2016). Magmatic oxygen fugacity estimated using zircon-melt partitioning of cerium. *Earth Planet. Sci. Lett.* 453, 260–266. doi:10.1016/j.epsl.2016.08.013

Sun, W., Huang, R. F., Li, H., Hu, Y. B., Zhang, C. C., Sun, S. J., et al. (2015). Porphyry deposits and oxidized magmas. *Ore Geol. Rev.* 65, 97–131. doi:10.1016/j.oregeorev.2014.09.004

Tramm, F., Wirth, R., Budzyń, B., Sláma, J., and Schreiber, A. (2021). LA-ICP-MS and TEM constraints on the magmatic and post-magmatic processes recorded by the zircon-xenotime intergrowth in pegmatite (Piława Górna, Góry Sowie Block, SW Poland). *Lithos* 404, 106480. doi:10.1016/j.lithos.2021.106480

van Staal, C. R., and Barr, S. M. (2012). Lithospheric architecture and tectonic evolution of the Canadian Appalachians and associated Atlantic margin. Chapter 2, in *Tectonic Styles in Canada: the lithoprobe perspective*. Editors J. A. Percival, F. A. Cook, and R. M. Clowes (Geological Association of Canada), 41–95. Special Paper. 49.

Wang, J., Wang, Q., Dan, W., Yang, J. H., Yang, Z. Y., Sun, P., et al. (2019). The role of clinopyroxene in amphibole fractionation of arc magmas: evidence from mafic intrusive rocks within the Gangdese arc, southern Tibet. *Lithos* 338, 174–188. doi:10.1016/j.lithos.2019.04.013

Whalen, J. B. (1993). Geology, petrography and geochemistry of Appalachian granites in New Brunswick and Gaspésie, québec. *Geol. Surv. Can. Bull.* 436, 130.

Whalen, J. B., Fyffe, L. R., Longstaffe, F. J., and Jenner, G. A. (1996a). The position and nature of the Gander–Avalon boundary, southern New Brunswick, based on geochemical and isotopic data from granitoid rocks. *Can. J. Earth Sci.* 33 (2), 129–139. doi:10.1139/e96-013

Whalen, J. B., and Hildebrand, R. S. (2019). Trace element discrimination of arc, slab failure, and A-type granitic rocks. *Lithos* 348, 105179. doi:10.1016/j.lithos.2019.105179

Whalen, J. B., Jenner, G. A., Currie, K. L., Barr, S. M., Longstaffe, F. J., and Hegner, E. (1994a). Geochemical and isotopic characteristics of granitoids of the Avalon Zone, southern New Brunswick: possible evidence for repeated delamination events. *J. Geol.* 102 (3), 269–282. doi:10.1086/629670

Whalen, J. B., Jenner, G. A., Hegner, E., Gariépy, C., and Longstaffe, F. J. (1994b). Geochemical and isotopic (Nd, O, and Pb) constraints on granite sources in the Humber and Dunnage zones, Gaspésie, Québec, and New Brunswick: implications for tectonics and crustal structure. *Can. J. Earth Sci.* 31 (2), 323–340. doi:10.1139/e94-030

Whalen, J. B., Jenner, G. A., Longstaffe, F. J., and Hegner, E. (1996b). Nature and evolution of the eastern margin of lapetus: geochemical and isotopic constraints from Siluro-Devonian granitoid plutons in the New Brunswick Appalachians. *Can. J. Earth Sci.* 33 (2), 140–155. doi:10.1139/e96-014

Whalen, J. B., Rogers, N., van Staal, C. R., Longstaffe, F. J., Jenner, G. A., and Winchester, J. A. (1998). Geochemical and isotopic (Nd, O) data from Ordovician felsic plutonic and volcanic rocks of the Miramichi Highlands: petrogenetic and metallogenic implications for the Bathurst Mining Camp. *Can. J. Earth Sci.* 35 (3), 237–252. doi:10.1139/e97-102

Yousefi, F., Lentz, D. R., McFarlane, C. R. M., Walker, J. A., and Thorne, K. G. (2023d). A Review of Geochronology of Devonian porphyries in New Brunswick and their relationship to Cu-Mo-Au porphyry style mineralization in this part of the northern Appalachians: comparison of existing ages and recent U-Pb titanite dating. In abstracts 2023. Exploration, Mining and Petroleum New Brunswick. *N. B. Dep. Nat. Resour. Energy Dev. Geoscience Rep. 2023*, 69.

Yousefi, F., Lentz, D. R., and Thorne, K. G. (2023a). Mineral chemistry of the Eagle Lake Granite porphyry, southwestern new Brunswick, Canada: implications for Cu-Mo-Au mineralization. *Can. J. Mineralogy Petrology* 61, 445–465. doi:10.3749/2200060

Yousefi, F., Lentz, D. R., Thorne, K. G., McFarlane, C. R. M., and Cousens, B. (2023b). Petrogenesis of the Eagle Lake Granite and associated Cu-Mo-Au mineralization, southwestern new Brunswick, Canada. *Minerals* 13, 1–29. doi:10.3390/min13050594

Yousefi, F., Lentz, D. R., and Walker, J. (2021). "Early Devonian Blue Mountain granodiorites and associated Benjamin River south porphyry Cu-Mo deposits, northeastern new Brunswick: analysis of adakitic signatures and fertility," in *Abstracts 2021: GAC-MAC* (London: Exploring Geosciences Through Times and Space), 1. Ontario 2021.

Yousefi, F., Lentz, D. R., Walker, J. A., and Thorne, K. G. (2022a). Overview of the Devonian porphyries with adakitic affinities in the northeastern Appalachians and their potential for Cu±Au±Mo mineralization. In abstracts 2022. Exploration, Mining and Petroleum New Brunswick. New Brunswick Department of Natural Resources and Energy Development, Geoscience Report 2022, p. 65.

Yousefi, F., Lentz, D. R., Walker, J. A., and Thorne, K. G. (2022b). An overview of the Devonian intrusive rocks in New Brunswick and their relationship to porphyry-style gold, copper, and molybdenum mineralization. In abstracts 2022. Prospectors and Developers Association of Canada ("PDAC"), Toronto, 2022, p. 1.

Yousefi, F., Lentz, D. R., Walker, J. A., and Thorne, K. G. (2024). Is the genesis of porphyry Cu-related adakitic rocks in New Brunswick, a result of slab failure? *Abstr. 2024 AGS Colloq. Monct.* 2024, 1.

Yousefi, F., White, T., Lentz, D. R., McFarlane, C. R., and Thorne, K. G. (2023c). Middle Devonian Evandale porphyry Cu-Mo (Au) deposit, southwestern New Brunswick, Canada: analysis of petrogenesis to potential as a source for distal intrusion-related epithermal gold mineralization. *Ore Geol. Rev.* 162, 105716. doi:10.1016/j.oregeorev.2023.105716